

# On the Use of Multipole Expansion in Time Evolution of Non-linear Dynamical Systems and Some Surprises Related to Superradiance<sup>‡</sup>

**Péter Csizmadia**<sup>1</sup>, **András László**<sup>1,2</sup>, **István Rácz**<sup>1</sup>

<sup>1</sup>WIGNER RCP, H-1121 Budapest, Konkoly-Thege Miklós út 29-33., Hungary

<sup>2</sup>CERN, CH-1211 Genève 23, Switzerland

E-mail: laszlo.andras@wigner.mta.hu, racz.istvan@wigner.mta.hu

**Abstract.** A new numerical method is introduced to study the problem of time evolution of generic non-linear dynamical systems in four-dimensional spacetimes. It is assumed that the time level surfaces are foliated by a one-parameter family of codimension two compact surfaces with no boundary and which are conformal to a Riemannian manifold  $\mathcal{C}$ . The method is based on the use of a multipole expansion determined uniquely by the induced metric structure on  $\mathcal{C}$ . The approach is fully spectral—i.e. it avoids pointwise evaluations of the basic variables—in the angular directions. Instead, Gaunt coefficients as matrix elements are used to evaluate multilinear expressions. The dynamics in the complementary 1+1 Lorentzian spacetime is followed by making use of a fourth order finite differencing scheme. In handling the pertinent 1+1 transverse degrees of freedom the techniques of adaptive mesh refinement (AMR) is also applied.

In checking the reliability and effectiveness of the introduced new method the evolution of a massless scalar field on a fixed Kerr spacetime is investigated. In particular, the angular distribution of the evolving field in superradiant scattering is studied. The primary aim was to check the validity of some of the recent arguments claiming that the Penrose process, or its field theoretical correspondence—superradiance—does play crucial role in jet formation in black hole spacetimes while matter accretes onto the central object. Our findings appear to be on contrary to these claims as the angular dependence of superradiant scattering of massless scalar fields does not show any preference of the axis of rotation. In addition, the characteristic properties of superradiance in case of a massless scalar field was also investigated. On contrary to the general expectations we found that by an incident wave packet, which had been tuned to be maximally superradiant, the acquired extra energy in the scattering process must be less than 0.1% of the energy sent in. It was found that instead of the occurrence of anticipated scale of energy extraction from black hole the to be superradiant part of the incident wave packet fail to reach the ergoregion rather it suffers a nearly perfect reflection which appears to be an interesting phenomenon.

PACS numbers: 04.25.D-

*Keywords:* multipole, spectral, non-linear, partial, differential, Gaunt, black hole, background, superradiance, Penrose process

<sup>‡</sup> This paper is dedicated to the memory of our friend Péter Csizmadia. Péter was a physicist, computer expert and one of the best Hungarian mountaineers. He disappeared in China's Sichuan near the Ren Zhong Feng peak of the Himalayas October 23, 2009. Péter was one of the founders and the main developer of our code GridRipper.

## 1. Introduction

The basic equations of various theories are non-linear. In studying these types of dynamical systems analytic methods by themselves do not provide a completely satisfactory framework. Therefore it seems to be of fundamental importance to develop numerical methods that are capable to simulate long time evolution of non-linear dynamical systems. Motivated by this sort of necessities in general relativity various groups developed their codes aiming to make progress in the study of astrophysical systems containing black holes and neutron stars. Fully general relativistic simulations of coalescing binaries consisting of neutron stars and/or black holes are now possible by making use of variants of the generalized harmonic formulation [1] and moving puncture approach [2, 3] in the Baumgarte-Shapiro-Shibata-Nakamura (BSSN) formalism [4, 5] (for a comprehensive review on the recent developments with additional references see, e.g., [6, 7]).

Besides these main stream efforts there are some apparently less ambitious ongoing projects trying to provide precise long term time evolution of various matter fields on fixed stationary background spacetimes which may or may not contain a black hole. In general, these investigations—due to the relative simplicity of the underlying physical system—provide an arena to test some of the new numerical methods before applying them to investigate the aforementioned much more complicated astrophysical systems. Immediate examples for these type of investigations with a stationary black hole as a background spacetime can be found, e.g. in [8] where high order finite differencing was applied, or in [9] where investigations of axial symmetric systems and the use of pseudospectral method (although only moderate angular momentum quantum numbers were involved), or in [10] where results on the use of pseudospectral method without assuming axial symmetry but with utilizing parallel computing were reported. Similar dynamical systems were investigated in a series of papers [11, 12, 13, 14, 15]. In these papers the viability of the simultaneous use of the techniques of conformal compactification, along with the use of hyperboloidal initial value problem, in numerical simulations were demonstrated.

In the present paper we introduce a numerical method to study the problem of time evolution of generic non-linear dynamical system in four-dimensional spacetimes. The time level surfaces are assumed to be foliated by a one-parameter family of codimension two surfaces which are conformal to a compact Riemannian manifold  $\mathcal{C}$  without boundary. The degrees of freedom in directions tangential to  $\mathcal{C}$ —they are referred as angular directions—are treated with spectral representation (multipole expansion whenever  $\mathcal{C}$  is homeomorph to a two-sphere  $\mathbb{S}^2$ ) which is based on  $L^2$  expansions of the basic variables in terms of the eigenfunctions of the Laplace operator on  $\mathcal{C}$ . The fields in the transverse 1+1 dimensional spacetime directions are evolved by making use of the method of lines based on a fourth order finite difference numerical scheme. The pertinent numerical method incorporates the techniques of the adaptive mesh refinement (AMR). All the operations on the basic variables, involving angular degrees of freedom,

are done without applying point-wise evaluations, i.e. the method is fully spectral, not pseudospectral.

There are various advantages ensured by this method. Firstly, the usual problems related to the coordinate singularities in the involved angular differential operators can be avoided. Secondly, all the operations in the angular directions which are linear in the basic field variables are exact. What is even more significant—by applying the Sobolev embedding theorem based arguments—all the non-linear operations such as pointwise multiplication or division by fields can also be treated within the spectral representation. The mathematical background of the applied new method—it is assumed to be known but seldom, if ever, collected in a systematic self contained way—is also presented in details in the appendices.

In practice, all the multipole expansion series are truncated at certain finite order. In this respect the applied method is perturbative. Nevertheless, the error introduced by these approximations can be kept to be at a tolerable low level by increasing the number of the involved modes. The residual error is monitored and the precision, efficiency and the viability of the proposed method have been justified to be satisfactory.

The introduced new method is applied to investigate the time evolution of a massless Klein-Gordon field on a fixed Kerr black hole spacetime. Within this setting, the angular dependence of the outgoing radiation was studied such that the initial data was fine tuned to have the highest possible potential for superradiance. Our investigations were motivated by some recent attempts trying to provide a physical model yielding high energy collimated matter streams (referred frequently as jets) originating from compact astrophysical objects.

For instance, in [16] it was asserted that Penrose process involving Compton scattering on electrons and electron-positron pair production in photon-photon scattering can give rise to ejection of highly collimated matter streams along the axis of rotation. In [17] an alternative support of these expectations was proposed. In particular, the possible existence of a class of timelike geodesics representing the worldline of the escaping particle yielded in the Penrose process—thereby emerging from the ergoregion—and having the axis of rotation of the black hole as an asymptote was examined. On contrary to these expectations in [18] where the evolution of a dust sphere falling onto a rotating black hole was considered no significant collimation effect had been found.

In the present paper an analogous field theoretical model will be investigated. Distinguished attention will be paid to the angular dependence of outgoing radiation yielded by a scattering process with using initial data that has been fine tuned to possess the highest possible potential to generate superradiance.

Let us also mention here that some preliminary studies of the dynamics of massless scalar field has been done by the present authors in [19] (see also [15]§). However, neither the initial condition was fine tuned to generate to be superradiant solution,

§ The code applied in [15] to study the long time evolution was developed essentially by reducing the complexity and by adopting the basic ideas of GridRipper [19, 20] to the investigated specific problem.

nor a detailed description of the applied numerical methods was given in either of these works. We would also like to emphasize that in parallel to the preparation this paper the corresponding package of GridRipper with the implementation of the system investigated in this paper is made to be available for public use [20].

Let us also recall here that, based on the estimates in [21, 22], superradiance is expected to be more significant whenever higher spin fields such as gravitational radiation is involved. Nevertheless, as stated above, throughout this paper considerations are restricted to the case of complex scalar fields. Similarly, our results concerning jet formation assume that the involved matter is modeled by a complex scalar field. Thereby our results do not exclude jet formation found in some recent astrophysically motivated more complex magnetohydrodynamical simulations (see e.g. [23, 24, 25]).

The paper is organized as follows. In Section 2 the physical setup including the field equations and coordinate choices are introduced. Section 3 to present an outline of the applied numerical method. Section 4 is to discuss some of the delicate issues related to the applied boundary conditions, while in Section 6 the initial data used in our numerical simulations is introduced. The main results are exposed in Section 7, while our concluding remarks are summarized in Section 8. The Appendices are to provide a systematic summary of the mathematical background of the applied new method, in particular, presenting all the details making it possible to use the techniques of multipole expansion in treatment of non-linear dynamical systems.

## 2. Field Equations

As mentioned above in this paper the evolution of a neutral massless scalar field propagating on the domain of outer communication of a fixed stationary Kerr black hole spacetime is considered. Although the code developed (which can be downloaded from [20]) is also capable to evolve a charged and self-interacting scalar field on a Kerr-Newman background in this paper attention will be restricted to the above mentioned simple case. We would like to mention that even this simple dynamical system is complex enough to test the viability and reliability of the proposed new method based on the spectral method.

To start off let us recall first the Kerr metric given in Boyer-Lindquist coordinates  $t, r, \vartheta, \varphi$  [27]. The part of the spacetime on which our investigations will be carried out is the domain of outer communication that possesses the product structure  $\mathbb{R}^2 \times \mathbb{S}^2$  and can be covered by Boyer-Lindquist coordinates  $t, r, \vartheta$  and  $\varphi$  taking values from the intervals  $-\infty < t < \infty$ ,  $0 < r < \infty$ ,  $0 \leq \vartheta \leq \pi$  and  $0 \leq \varphi \leq 2\pi$ . The metric  $g$  in these coordinates reads as

$$g = -\frac{\Delta - a^2 \sin^2(\vartheta)}{\Sigma} dt \otimes dt - \frac{a(r^2 + a^2 - \Delta) \sin^2(\vartheta)}{\Sigma} (dt \otimes d\varphi + d\varphi \otimes dt)$$

$$+ \frac{\Sigma}{\Delta} dr \otimes dr + \Sigma d\vartheta \otimes d\vartheta + \frac{\Gamma \sin^2(\vartheta)}{\Sigma} d\varphi \otimes d\varphi, \quad (2.1)$$

where the smooth functions  $\Delta$ ,  $\Sigma$  and  $\Gamma$  are determined by the relations

$$\begin{aligned} \Delta &= r^2 + a^2 - 2Mr, \\ \Sigma &= r^2 + a^2 \cos^2(\vartheta), \\ \Gamma &= (r^2 + a^2)^2 - a^2 \Delta \sin^2(\vartheta). \end{aligned} \quad (2.2)$$

The symbols  $M$  and  $a$  denote the mass and the specific angular momentum of the Kerr black hole spacetime. The field equation of a complex valued scalar field  $\Phi$  can be written as

$$\nabla^a \nabla_a \Phi = 0, \quad (2.3)$$

which after the conventional first order reduction, for the vector variable  $(\Phi, \Phi_t, \Phi_r)^T$ , reads as

$$\begin{aligned} \partial_t \Phi &= \Phi_t, \\ \partial_t \Phi_t &= \frac{1}{\Gamma} \left( \Delta^2 \partial_r \Phi_r + 2\Delta(r-M)\Phi_r + \Delta \mathbb{L}_{\mathbb{S}^2}(\Phi) \right. \\ &\quad \left. - a^2 \partial_\varphi^2 \Phi - 2a(r^2 + a^2 - \Delta) \partial_\varphi \Phi_t \right), \\ \partial_t \Phi_r &= \partial_r \Phi_t \end{aligned} \quad (2.4)$$

where the differential operator

$$\mathbb{L}_{\mathbb{S}^2} = \frac{1}{\sin \vartheta} \partial_\vartheta [\sin \vartheta \partial_\vartheta] + \frac{1}{\sin^2 \vartheta} \partial_\varphi^2 \quad (2.5)$$

is nothing but the Laplace operator on the unit sphere  $\mathbb{S}^2$  with its canonical Riemann metric. To get rid of the coordinate singularity of the radial differential operator for the first multipole component of  $\Phi$  at the origin in the Minkowski limit—that can also be applied in other cases whenever an origin is present in the computational domain—the following conventional trick had been applied. Instead of  $\Phi$  the variable  $\Psi = r \cdot \Phi$  was evolved using the field equation transformed accordingly.

In the Kerr case with  $M > 0$  it turned to be rewarding to use instead of the  $r$  and  $\varphi$  the new ones  $r_*$  and  $\tilde{\varphi}$  defined as

$$r_*(r) = r + \frac{1}{2} \left( \frac{\ln(r - r_+)}{\kappa_+} + \frac{\ln(r - r_-)}{\kappa_-} \right), \quad (2.6)$$

$$\tilde{\varphi}(r, \varphi) = \varphi + \frac{a}{r_+ - r_-} \ln \left[ \frac{r - r_+}{r - r_-} \right], \quad (2.7)$$

where

$$\kappa_\pm = \frac{1}{2} \frac{r_\pm - r_\mp}{r_\pm^2 + a^2} \quad (2.8)$$

is the surface gravity on the outer and inner event horizon located at  $r_\pm = M \pm \sqrt{M^2 - a^2}$ , respectively. By making use of these coordinates close to the event horizon much better resolution could be achieved which is supported by the fact that the null geodesics of minimal impact can be given as  $t \pm r_* = \text{const}$ ,  $\vartheta = \text{const}$ ,  $\tilde{\varphi} = \text{const}$ .

In consequence of the use of these new coordinates during the evaluation the inverse relation  $r = r(r_*)$  had to be determined numerically which was done by implementing a simple Newton-Raphson method.

### 3. Numerical Evolution

This Section is to provide a short outline of the applied numerical methods. As mentioned already the method is based on multipole expansion on each of the topological two-spheres determined by the  $t = \text{const}$  and  $r = \text{const}$  level surfaces. Accordingly, instead of evolving the fields  $\Phi$ ,  $\Phi_t$  and  $\Phi_{r_*}$  themselves their multipole components  $[\Phi]_\ell^m$ ,  $[\Phi_t]_\ell^m$  and  $[\Phi_{r_*}]_\ell^m$ —which are functions of  $t$  and  $r_*$  exclusively yielded by  $L^2$  expansions of  $\Phi$ ,  $\Phi_t$  and  $\Phi_{r_*}$  with respect to the spherical harmonics—

$$\{Y_\ell^m | \ell = 0, \dots, \infty, m = -\ell, \dots, \ell\}, \quad (3.1)$$

had been evolved. A comprehensive presentation of the mathematical background can be found in the Appendices, while the applied code GridRipper with the implementation of the investigated system can be found at [20].

#### 3.1. Evolution in the $t, r$ section

The evolution equations for the multipole components  $[\Phi]_\ell^m$ ,  $[\Phi_t]_\ell^m$  and  $[\Phi_{r_*}]_\ell^m$  were solved in the  $t - r_*$  plane by making use of the 1+1 dimensional C++ based PDE solver of GridRipper described in details in [29, 30, 20]. The numerical algorithm utilized by this code is based on the method of lines in a fourth order Runge-Kutta scheme such that the spatial derivatives were evaluated with a fourth order symmetric finite difference stencil. To guarantee stability—by suppressing high frequency instabilities—a standard fifth order dissipation term, as proposed by Gustafsson et al [26] was also applied in solving the evolution equations for the multipole components  $[\Phi]_\ell^m$ ,  $[\Phi_t]_\ell^m$  and  $[\Phi_{r_*}]_\ell^m$ . Note, that the use of this dissipation term does not affect the order of accuracy of the applied numerical scheme.

The 1+1 algorithm of GridRipper makes use, as a built in package, the techniques of adaptive mesh refinement (AMR) as proposed by Berger-Oliger algorithm [31] (see also [30, 29]). The use of AMR is based on the idea that a refining of the spacetime mesh has to be done at those locations where the Richardson error

$$\frac{\|f_{\Delta t, \Delta r}(t, r) - f_{2\Delta t, 2\Delta r}(t, r)\|}{2\Delta t (2^q - 1)} \quad (3.2)$$

exceeds a predefined threshold, where  $f_{\Delta t, \Delta r}$  denotes the numerical solution obtained on a spacetime mesh with  $\Delta t$  temporal and  $\Delta r$  spatial finite difference,  $q$  is the order of accuracy of the finite difference scheme, and  $\|\cdot\|$  is a semi-norm. As spatial and temporal refinement is performed simultaneously, the value of the Courant factor—i.e., the ratio of the temporal and spatial step size—remains intact, thereby in principle the stability of the finite difference scheme is not affected.

In our simulations  $q$  took the value 4, while the semi-norm  $\|\cdot\|$  was chosen to be the  $L^2$  norm of the multipole expansion of  $\partial_{r_*}\Psi$  on each two-sphere. In order to be able to implement a relative error type quantity in specifying the tolerable error this  $L^2$  norm of  $\partial_{r_*}\Psi$  was normalized by the pertinent  $L^2$  norm of  $\partial_{r_*}\Psi$  on the initial slice.

### 3.2. Evolution in the angular $\vartheta, \tilde{\varphi}$ section

The remaining angular  $\vartheta, \tilde{\varphi}$  directions were handled by a purely spectral method, completely avoiding point evaluation. The expansion coefficients  $[\Phi]_\ell^m$ ,  $[\Phi_t]_\ell^m$  and  $[\Phi_{r_*}]_\ell^m$  were stored in a C++ structure implementing an algebra defined by coefficient-wise linear operations and with pointwise multiplication of the basic variables. It is worth to be emphasized that the viable utility of the latter operation is not obvious at all as the multipole series, by construction, are guaranteed to be convergent only in the  $L^2$  sense without an immediate support of their convergence in the pointwise sense. Therefore, in the generic case, the multipole expansion coefficients of pointwise products are not expected to be derived from the multipole coefficients of the factors without evaluating them pointwise and applying a subsequent numerical multipole expansion of the yielded product. Clearly, such a complicated approach would be computationally intensive not allowing the use of multipole expansions with sufficiently large  $\ell$  values, e.g.  $\ell \geq 16$ , to make the error introduced by truncation to be tolerably small. Nevertheless, whenever the basic variables are known to belong to the class of  $C^2$  functions there exists a purely spectral approach that makes the evaluation of their pointwise multiplication possible. All of the underlying ideas—which are of fundamental importance in guaranteeing the effectiveness of the proposed new method—are justified with mathematical rigor in Appendix A and Appendix B. It is worth to be noted that every solution to a field equation involving second derivatives in the strong sense is of differentiability class  $C^2$ . As the proposed use of the spectral method avoids pointwise evaluations there is a significant reduction in the required computational power in carrying out full 3+1 dimensional simulations. This reduction is also supported by the fact that the Gaunt coefficients, introduced in Appendix B, which are necessary in evaluating products of multipole coefficients have to be calculated only once and stored them in the computer memory during the rest of the simulation.

In practice, whenever pointwise products of  $C^2$  fields truncated at  $\ell_1$  and  $\ell_2$  multipole order is evaluated the result shall have non-vanishing coefficients up to  $\ell_1 + \ell_2$  multipole order. Therefore, as opposed to linear operations, multiplications do not respect any prefixed maximal expansion order. Correspondingly, in the applied numerical approximation the multipole order of products have to be kept to be bounded which was done by truncating at the value  $\max(\ell_1, \ell_2)$ . Note, however, that convergence tests have to be performed by varying the maximal allowed order  $\ell_{\max}$  to justify the viability and the accuracy of the proposed numerical scheme.

In evaluating the time derivative of the basic variables another critical non-linear operation has also to be performed. It is the division by a nowhere vanishing variable.

The associated difficulties can be overcome by tracing back the operation of pointwise division to the operation of pointwise multiplication with the help of Neumann series expansions. This perturbative method as discussed in details in Appendix C and Appendix D as it is another key ingredient of the proposed new method. It is also shown there that the necessary number of iterations in performing this perturbative division method grows only with the logarithm of the required accuracy.

### 3.3. Storage and computational requirements

The storage of the basic variables via their multipole coefficients becomes even more efficient when the variables may be assumed to be of  $C^\infty$  class in the angular directions as in that case the corresponding sequence of multipole expansion coefficients are guaranteed to decay faster than any polynomial order as it is justified in Appendix E. The number of non-vanishing multipole coefficients of a variable, truncated at maximal order  $\ell_{\max}$ , is  $(\ell_{\max} + 1)^2$ . Therefore, the storage requirement is quadratic in  $\ell_{\max}$ . For the number of the non-zero Gaunt coefficients the approximate formula  $0.7 \cdot (\ell_{\max})^{4.7}$  can be verified numerically for  $\ell_{\max} \geq 8$ . In particular, if the considered problem is axially symmetric the number of non-zero multipole coefficients is only  $\ell_{\max} + 1$ , while the number of Gaunt coefficients necessary to evaluate non-linear terms scale as  $0.66 \cdot (\ell_{\max})^{2.8}$  provided that  $\ell_{\max} \geq 8$ .

It is also informative to compare the computational expense estimates to that of other widely used methods, for instance pseudospectral methods. These store field values over coordinate grids, but evaluate spatial/angular derivatives in the spectral representation. In case of applying the most commonly used basis, the Chebyshev polynomials and storing field values over the set of Gauss-Lobatto collocation points, one faces the problem of regularizing the coordinate singularities of the spherical Laplace operator. In order to avoid the associated difficulties, it is quite natural to choose more suitable expansion basis, namely spherical harmonics—similarly as in our proposed method. In adopting this strategy, one must do conversion between grid values and spectral coefficients. In order to estimate the cost of such operation, one has to take into account that at each mesh point a sum over the indices  $\ell$  and  $m$  has to be performed. For each mesh point in the  $\vartheta$  angle coordinate a sum over the index  $\ell$ , with evaluations for the involved  $m$  values, consists of  $(\ell_{\max} + 1)^2$  terms. In addition, the cost of a sum over of the  $m$  values—which may be evaluated by making use of fast Fourier transform—can be seen to go not better than  $5(2\ell_{\max} + 1) \log_2(2\ell_{\max} + 1)$ . Taking then into account that there exists  $\ell_{\max} + 1$  pieces of mesh points in  $\vartheta$ , as a minimal estimate of the total cost of a (non-approximate) spectral transformation in a pseudospectral method we get  $5(\ell_{\max} + 1)^3(2\ell_{\max} + 1) \log_2(2\ell_{\max} + 1)$ . On the other hand, the evaluation of non-linear terms using matrix products in our method scales as  $\sim 0.7 \cdot (\ell_{\max}^{4.7})$ . Therefore, the computational costs of these two methods appear to be comparable although in the range  $8 \leq \ell_{\max} \leq 32$  there is about factor of ten preference on the side of the fully spectral method. Clearly, at the end of the simulation we also need to do pointwise evaluations



in extracting the physical content of the yielded data. However, these evaluations need not to be done on each time level surfaces rather only at some specific ones. A slight additional advantage is that the involved vast number of matrix multiplications in the spectral case can be paralellized in a very effective way. Nevertheless, we admit that it is really the physical problem which should decide which method fits better.

#### 4. Boundary Conditions

The proper treatment of the timelike part of the boundaries is of fundamental importance in both analytic and numerical evolutionary problems [32, 33, 34, 35]. On numerical side it is only a tiny technical part of the problem that the spatial derivatives cannot be evaluated by making use a symmetric stencil close and at the boundary. The major part of the problems originates from the fact that there remains a freedom in specifying free data on the timelike part of the boundary [32, 33].

In numerical approaches one of the most conventional treatment is to use the Sommerfeld outgoing radiation boundary condition. This method is based on the assumption that at the border the transformed variable  $\Psi = r \cdot \Phi$  has vanishing derivative along the outgoing radial null geodesics, which determines the value of  $\Psi_t$ , at the boundary, in terms of the values of  $\Psi$  and  $\Psi_r$  there. Note first that—given the simple form of the outgoing radial null geodesics in the Kerr spacetime in terms of the  $t, r_*$  coordinates [28]—it is straightforward to implement this boundary condition in our numerical setup based on the spectral method. Nevertheless, in our first test runs the Sommerfeld boundary condition was found to yield unsatisfactory behavior in long term evolutions. One should keep in mind that even in the simple case of a scalar field on Minkowski background, in case of a non-spherical field configurations, only a much more sophisticated treatment [36] can provide a proper numerical treatment, and this approach does not generalize—at least not in a straightforward way—to more general background spacetimes such as the Kerr black hole. In virtue of this result one does not expect the Sommerfeld outgoing radiation boundary condition to work properly. Indeed, it was shown in [34, 37] that even in the simplest possible case of a massless Klein-Gordon field in Schwarzschild spacetime the asymptotic decay rate of the field may significantly be affected by the use of the Sommerfeld boundary condition. Our numerical experiments also justified (see Figure 4.1 below) that this outgoing radiation condition yields to significant instabilities at the boundary even in the short-term evolution of strongly non-spherically symmetric configurations.

Another obvious idea is to carry out the numerical simulation near the boundary may be the following. Instead of applying any sort of outgoing radiation condition use the fourth order method of lines everywhere—as it is done in the interior—by making use of an asymmetric stencil close and at the boundaries. This simple minded approach also yields instabilities developing at the boundaries, although this occurs much later than in case of the Sommerfeld boundary condition. These type of instabilities most likely are consequences of the sum up of the error produced by the asymmetric fourth order

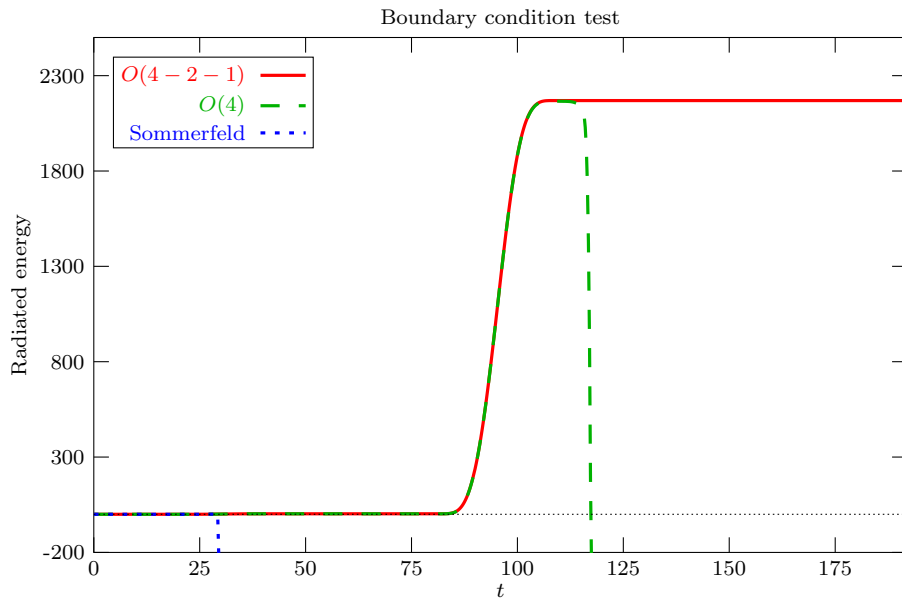
stencils close and at the boundaries. While trying to cure this unfavorable behavior we invented the following simple trick. The order of the finite difference scheme was gradually decreased from 4 to 2 then to 1 such that we still had fourth order symmetric scheme at the last but two points, second order symmetric schemes at the last but one points and a first order upstream or downstream at the right or left boundaries, respectively. The first order asymmetric treatment at the boundaries could also be considered as a simultaneous combination of a linear extrapolation of the field variable next to the boundary point with the application of a second order symmetric differential scheme. Numerical experiments justified that this simple trick in evaluating the spatial derivatives close and at the boundaries—although with the price of a reduction of the numerical convergence rate there—stabilized the time evolution and, more importantly, guaranteed a long term satisfaction of the energy balance relation even for the evolution of non-spherically symmetric field configurations.

Figure 4.1 shows a comparison of the effectiveness of the Sommerfeld boundary condition, the simple  $O(4)$  boundary condition—with fourth order asymmetric stencil close and at the boundary—and the developed  $O(4 - 2 - 1)$  boundary condition—where the order of the finite difference scheme was gradually decreased from 4 to 2 then to 1—as described in details above. In particular, the time evolution of a rotating massless scalar field with a solid toroidal support is considered, by using either of these three boundary conditions, on Minkowski background. It can be seen that the energy outflow pattern at the outer boundary, located at  $r = 63$ , remains, in long term evolution, according to our expectations only for the case of  $O(4 - 2 - 1)$  boundary condition. In the other two cases so much spurious energy flows back into the computational domain through the outer boundary that kills the evolution at  $t \sim 26$  for the Sommerfeld boundary condition and at  $t \sim 100$  for the  $O(4)$  boundary condition.

It is of obvious interest to know whether the  $O(4 - 2 - 1)$  “boundary condition” proposed and used by us is a proper one. A sufficiently detailed investigation of this issue exceeds the frame of the present paper and the pertinent results will be published elsewhere. Nevertheless, a simpleminded explanation concerning the well-posedness of the associated initial-boundary-value problem will be given below. Before doing so let us point to some of the most fundamental facts which should also support our claim that the proposed  $O(4 - 2 - 1)$  differential scheme does impose proper boundary conditions.

- (1) While by applying the Sommerfeld condition the code crashes faster than in case of the  $O(4)$  schema where no boundary condition at all had been applied. As opposed to this long term stability characterizes the use of  $O(4 - 2 - 1)$  differential scheme.
- (2) The exponential convergence rate, along with the high precession of the energy and angular momentum balances (see Section 7), could not be achieved without propagating all the physical modes towards the boundary such that they leave the computational domain without reflection, i.e., no spurious incoming modes are born at the boundaries.

The simpleminded argument goes as follows: Assume that we have a first order



**Figure 4.1.** (Color online) The energy outflow as a function of temporal coordinate  $t$  at the outer boundary, located at  $r = 63$ , for the evolution of an initially rotating massless scalar field on Minkowski background is shown with the application of the Sommerfeld,  $O(4)$  and  $O(4 - 2 - 1)$  boundary conditions, respectively. It can be seen that in case of Sommerfeld or  $O(4)$  boundary conditions a spurious energy flow back, from the outer boundary, occurs, while no such spurious energy flow back happens in case of the  $O(4 - 2 - 1)$  boundary condition. These numerical investigations were carried out using  $\ell_{\max} = 12$  and 512 spatial points in the base grid such that  $n = 5$  AMR refinement levels were allowed.

system of hyperbolic field equation of the form  $u_t = Au_r + Bu$  for a vector valued field variable  $u$ . In applying the  $O(4 - 2 - 1)$  scheme at the last grid point a first order downstream finite difference stencil is applied. This, however, can be seen to be equivalent to the application of a second order symmetric finite difference stencil combined with a linear extrapolation. These two operations guarantee that the second  $r$ -derivative,  $u_{rr}$ , vanishes there. This, in virtue of this field equation, yields a mild restriction—of the type applied in Sections 9-11 of [26]—on the  $t$ -derivative,  $u_t$ , at the very last grid point, in spite of the fact that apparently only the field equations were imposed there.

## 5. Treatment of an origin

The presence of an origin on the time slices always requires a very careful and precise treatment. An origin shows up in various physically realistic situations. For instance, if the background is the Minkowski spacetime or in case of fully dynamical spacetimes containing a pulsating neutron star. It worth to be emphasized that the method outlined below is applicable not only in case of a Minkowski background but in the generic case of fully dynamical spacetimes, as well.

Before proceeding note that in the fully dynamical situations the time slices might contain more than one origin or no origin at all (see, e.g. [38] for explicit examples).

Nevertheless, in this Section attention will be restricted to the conventional single origin case. In order to avoid ambiguities the  $r$ -coordinate is arbitrary and the origin is assumed to be located at  $r = 0$ .

In order to avoid the appearance of the usual  $r$ -coordinate singularity in evaluating the radial part of the Laplace operator at the origin, the new basic variable  $\Psi = r \cdot \Phi$  has already been introduced. Whenever an origin is located at  $r = 0$  a symmetric fourth order stencil can be applied in determining the spatial derivatives at and in a neighborhood of the origin based on the observation that the multipole coefficients  $[\Psi]_\ell^m$  may formally be extended to negative radii according to the rule

$$[\Psi]_\ell^m(-r) = (-1)^{\ell+1}[\Psi]_\ell^m(r). \quad (5.1)$$

This relation follows from the assumption that the original field variable  $\Phi$  is at least  $C^1$ —thereby it is  $C^1$  along arbitrary straight lines through the origin—and from the reflection property of the spherical harmonics  $Y_\ell^m$  under the transformation  $\vartheta, \varphi \mapsto \pi - \vartheta, \varphi + \pi$ .||

In addition, if  $\Phi$  is assumed to be  $C^2$ —this assumption should not be considered as extreme especially if one recalls that  $\Phi$  is subject to (2.3)—its spatial Laplacian

$$\frac{1}{r} \partial_r^2(r \cdot \Phi) + \frac{1}{r^2} \mathbb{L}_{\mathbb{S}^2}(\Phi) \quad (5.2)$$

has to be finite at the origin. From this, along with subsequent applications of l'Hopital rule, the relations

$$\begin{aligned} \ell = 0 : \quad & \partial_r[\Phi]_\ell^m = 0, \\ \ell = 1 : \quad & [\Phi]_\ell^m = 0, \\ \ell \geq 2 : \quad & [\Phi]_\ell^m = 0, \quad \partial_r[\Phi]_\ell^m = 0 \end{aligned} \quad (5.3)$$

follow. This, however, along with the substitution  $\Psi = r \cdot \Phi$ , implies that the relations

$$\begin{aligned} \ell = 0 : \quad & [\Psi]_\ell^m = 0, \quad \partial_r^2[\Psi]_\ell^m = 0, \\ \ell = 1 : \quad & [\Psi]_\ell^m = 0, \quad \partial_r[\Psi]_\ell^m = 0, \\ \ell \geq 2 : \quad & [\Psi]_\ell^m = 0, \quad \partial_r[\Psi]_\ell^m = 0, \quad \partial_r^2[\Psi]_\ell^m = 0 \end{aligned} \quad (5.4)$$

hold for the multipole components  $[\Psi]_\ell^m$  at the origin.

In consequence of the algebraic relations  $[\Psi]_\ell^m = 0$  and  $\partial_r[\Psi]_\ell^m = 0$ , these hold for  $\ell \neq 0$  at the origin, the field equations read there as

$$\begin{aligned} \partial_t[\Psi]_\ell^m &= 0, \\ \partial_t[\Psi_t]_\ell^m &= 0, \end{aligned}$$

|| Indeed, the radial derivative  $\partial_r \Phi$  of  $\Phi(r, \vartheta, \varphi)$  corresponds to the directional derivative of  $\Phi$  along the radial direction characterized by the certain constant values of the angles  $\vartheta, \varphi$ . As  $\Phi$  is required to be  $C^1$ , the directional derivative  $\partial_r \Phi$  may, then, be numerically evaluated by making use of a symmetric stencil of the applied finite difference scheme such that values of  $\Phi$  from both sides of the origin are used at and closed to the origin. Nevertheless, on the the opposite side the values of  $\Phi$  can be determined as  $\Phi(r, \pi - \vartheta, \varphi + \pi) = \sum_{\ell=0}^{\infty} \sum_{m=-\ell}^{\ell} \Phi_\ell^m(r) Y_\ell^m(\pi - \vartheta, \varphi + \pi) = \sum_{\ell=0}^{\infty} \sum_{m=-\ell}^{\ell} \Phi_\ell^m(r) (-1)^\ell Y_\ell^m(\vartheta, \varphi)$ . Thus, by formally extending the functions  $\Phi_\ell^m$  to negative radii—by making use of the rule  $\Phi_\ell^m \mapsto (-1)^\ell \Phi_\ell^m$ —the radial derivative  $\partial_r \Phi_\ell^m$  of the functions  $\Phi_\ell^m$  can numerically be evaluated.

$$\partial_t[\Psi_r]_\ell^m = \begin{cases} \partial_r[\Psi_t]_\ell^m, & \text{if } \ell = 0 \\ 0, & \text{otherwise,} \end{cases} \quad (5.5)$$

which are completely regular at  $r = 0$ . In spite of this apparently straightforward regularization of the singular terms at the origin a simpleminded numerical implementation of (5.5) still yield unstable evolutions for non-spherically symmetric configurations. A close look at the evolution justifies that numerical error starts to grow very quickly at the grid-point next to the origin. This can be understood by recalling that in the evaluation of the ‘0/0’ type term

$$\frac{1}{r^2} \mathbb{L}_{\mathbb{S}^2}(\Psi) \quad (5.6)$$

the higher multipole components acquire larger weight, which significantly magnifies the related numerical error. Nevertheless, this difficulty can also be overcome by a systematic application of the algebraic relations formulated by (5.1) and (5.4). By requiring these conditions to hold—where the first and second derivatives are assumed to be evaluated as dictated by the applied fourth order symmetric finite difference scheme—it turns out that the values of  $[\Psi]_\ell^m$  at the origin and next to the origin are algebraically determined by the values of  $[\Psi]_\ell^m$  next to next to the origin, with the only exception  $[\Psi_r]_0^0$  which evolves according to the regular field equation  $\partial_t[\Psi_r]_0^0 = \partial_r[\Psi_t]_0^0$  [see (5.5)] at  $r = 0$ .

## 6. Initial Data and the Applied Grid

A generic initial data specification to our evolution equations (2.4) is composed by three functions  $\phi$ ,  $\phi_t$  and  $\phi_r$  specified on the  $t = 0$  initial data hypersurface, denoted by  $\Sigma_0$ , such that beside the trivial constraint  $\phi_r = \partial_r\phi$  for the corresponding solution  $\Phi$  the relations  $\Phi|_{\Sigma_0} = \phi$  and  $\Phi_t|_{\Sigma_0} = \phi_t$  also hold. It is straightforward to recast such an initial data specification for the rescaled field variable  $\Psi = r \cdot \Phi$  which is given as a function of the coordinates  $t, r_*, \vartheta, \varphi$  defined in Section 2.

### 6.1. Superradiance

Before proceeding and introducing our choice for the only freely specifiable functions  $\psi$  and  $\psi_t$  on  $\Sigma_0$  let us recall some simple facts related to superradiance. First of all, as it was shown first by Carter in [39] in the coordinates  $t, r_*, \vartheta, \varphi$  the d’Alembert operator separates for the  $t$ -Fourier transformed field. More precisely, the temporal Fourier transform,  $\mathcal{F}\Phi$ , of a solution  $\Phi$  to (2.4) may be decomposed as

$$\mathcal{F}\Phi(\omega, r_*, \vartheta, \varphi) = \frac{1}{\sqrt{r^2 + a^2}} \sum_{\ell=0}^{\infty} \sum_{m=-\ell}^{\ell} R_{\ell,\omega}^m(r_*) S_{\ell,a\omega}^m(\vartheta, \varphi), \quad (6.1)$$

where  $\omega$  is the frequency in the time translation direction and  $S_{\ell,a\omega}^m$  denotes the oblate spheroidal harmonic function with oblateness parameter  $a\omega$  and with angular

momentum quantum numbers  $\ell, m$ —they are eigenfunctions of a self-adjoint operator—, while for the radial functions  $R_{\ell,\omega}^m$  a one-dimensional Schrödinger equation of the form

$$\frac{d^2 R_{\ell,\omega}^m}{dr_*^2} + \left[ \left( \omega - \frac{ma}{r^2 + a^2} \right)^2 + \Delta \cdot V_{\ell,\omega}^m(r_*) \right] R_{\ell,\omega}^m = 0, \quad (6.2)$$

with suitable real potentials  $V_{\ell,\omega}^m(r_*)$  can be derived from the field equation (2.4).

The conventional argument ending up with the phenomenon called superradiance goes as follows. Physical solutions to (6.2) are supposed to possess the asymptotic behavior

$$R_{\ell,\omega}^m \sim \begin{cases} e^{-i\omega r_*} + \mathcal{R} e^{+i\omega r_*} & \text{as } r \rightarrow \infty \\ \mathcal{T} e^{-i(\omega - m\Omega_H)r_*} & \text{as } r \rightarrow r_+ \end{cases} \quad (6.3)$$

where  $\Omega_H$  denotes the angular velocity of the black hole with respect to the asymptotically stationary observers [27], and with reflection and transmission coefficients,  $\mathcal{R}$  and  $\mathcal{T}$  [42], respectively. Notice that this asymptotic behavior (6.3) presumes the existence of a transmitted wave submerging into the ergoregion. By evaluating the Wronskian of the corresponding fundamental solutions, “close” to infinity and “close” to the horizon, it can be shown that the reflection and transmission coefficients satisfy the relation  $(\omega - m\Omega_H) |\mathcal{T}|^2 = (1 - |\mathcal{R}|^2)\omega$  [44]. Thereby, whenever  $|\mathcal{R}| > 1$ —or equivalently, whenever  $|\mathcal{T}|$  does not vanish and the inequality  $0 < \omega < m\Omega_H$  holds—positive energy is supposed to be acquired by the backscattered scalar wave due to its interaction with the Kerr black hole in the ergoregion. This phenomenon is referred as superradiant scattering which is also known as the field theoretical correspondence of the Penrose process derived in context of point particle mechanics [40].

## 6.2. Initial data

In applying the introduced new numerical method our primary interest was to study the angular dependence of superradiant scattering. The applied initial data was specified accordingly—by applying an approach analogous to that of [41, 42]—and it was fine tuned to maximize the effect of superradiance.

However, to investigate a clear manifestation of superradiance in a fully dynamical process—i.e. the way an incident scalar wave acquires extra energy by submerging into the ergoregion and then carrying it away from the central region—the initial data we applied is of compact support such that it is separated from the ergoregion on the initial time slice. Thereby, the initial data we have applied differs significantly, in its fundamental character, from that of [41, 42]. To fulfill the above mentioned requirements the initial data for the rescaled field variable  $\Psi = r \cdot \Phi$  was chosen as

$$\begin{aligned} \psi(r_*, \vartheta, \tilde{\varphi}) &= e^{-i\omega_0(r_* - r_{*0})} f(r_* - r_{*0}) Y_\ell^m(\vartheta, \tilde{\varphi}), \\ \psi_t(r_*, \vartheta, \tilde{\varphi}) &= -i\omega_0 \psi(r_*, \vartheta, \tilde{\varphi}) + e^{-i\omega_0(r_* - r_{*0})} f'(r_* - r_{*0}) Y_\ell^m(\vartheta, \tilde{\varphi}), \\ \psi_{r_*}(r_*, \vartheta, \tilde{\varphi}) &= \partial_{r_*} \psi(r_*, \vartheta, \tilde{\varphi}), \end{aligned} \quad (6.4)$$

where  $f : \mathbb{R} \rightarrow \mathbb{C}$  is a smooth function of compact support,  $f'$  denotes its first derivative and  $\omega_0, r_{*0}$  are some real parameters. Note that the appearance of the extra  $r$  factor in  $\Psi$

has no effect on the above recalled argument concerning the appearance of superradiance. Indeed, this factor may be suppressed by redefining the function  $f$  that has not been specified yet.

It can be seen that in an asymptotic region of the Kerr background (or everywhere if the background is the Minkowski spacetime) the initial data specification (6.4) yields an inward traveling spherical wave packet starting with a radial profile  $f(r_* - r_{*0})$ . Accordingly, in an asymptotic region the solution in a sufficiently small neighborhood of the initial data surface might be approximated as

$$\Psi(t, r_*, \vartheta, \tilde{\varphi}) \approx e^{-i\omega_0(r_* - r_{*0} + t)} f(r_* - r_{*0} + t) Y_\ell^m(\vartheta, \tilde{\varphi}). \quad (6.5)$$

It is informative to have a look at the temporal Fourier transform,  $\mathcal{F}\Psi$ , of this approximate solution  $\Psi$  that reads as

$$\mathcal{F}\Psi(\omega, r_*, \vartheta, \tilde{\varphi}) \approx e^{-i\omega(r_* - r_{*0})} \mathcal{F}f(\omega - \omega_0) Y_\ell^m(\vartheta, \tilde{\varphi}), \quad (6.6)$$

where  $\omega$  being the temporal frequency while  $\mathcal{F}f$  stands for the Fourier-transform of  $f$ . Assuming that  $\mathcal{F}f$ —playing the role of a frequency profile function—is sufficiently narrow the approximate solution (6.5) looks almost like a monochromatic spherical wave solution similar in nature to the ingoing part of the wave determined by relations (6.1) and (6.3). Accordingly, by tuning  $\omega_0$  such that the energy flux absorbed by the black hole to become negative—this is expected to be achieved by choosing  $\omega_0$  such that  $0 < \omega_0 < m\Omega_H$ —one would expect that a to be superradiant solution is yielded. It can also be seen that the energy extraction may be maximized by choosing  $\omega_0 = \frac{1}{2}m\Omega_H$  and, in addition, by guaranteeing that  $\int_0^{m\Omega_H} |\mathcal{F}f|^2(\omega - \omega_0) d\omega \approx \int_{-\infty}^{\infty} |\mathcal{F}f|^2(\omega - \omega_0) d\omega$ , which happens whenever the frequency spectrum is narrow enough to be entirely included by the superradiant frequency regime.

We would like to emphasize that the above outlined construction of a to be superradiant initial data specification involves a number of heuristics assumptions. For instance, the Fourier spectrum (6.6) is assumed to represent the Fourier transform of the purely inward traveling wave (6.5) and whence the contribution from back scattering is completely neglected. To convince ourselves, in investigating the time evolutions of specific initial data choices, the power spectrum in temporal frequency of a supposed to be superradiant solution was also determined at a constant  $r_*$  sphere which is located towards the black hole with respect to the compact support of the initial data. As it can be seen on Figure 7.6 the solution remains in the desired frequency regime.

Based on the above outlined reasoning in our numerical simulations the radial profile function  $f : \mathbb{R} \rightarrow \mathbb{C}$  was chosen to possess the form

$$f_w(x) = \begin{cases} e^{\left[-\left|\frac{w}{x+\frac{w}{2}}\right| - \left|\frac{w}{x-\frac{w}{2}}\right| + 4\right]}, & \text{if } x \in \left[-\frac{w}{2}, \frac{w}{2}\right] \\ 0, & \text{otherwise,} \end{cases} \quad (6.7)$$

which is a smooth function of the real variable  $x$  with compact support  $\left[-\frac{w}{2}, \frac{w}{2}\right]$ . To be compatible with our most important physical requirements that yields an incident wave packet that may acquire extra energy after penetrating through the ergoregion the

initial parameter  $r_{*0}$  in (6.4) was chosen to be sufficiently large to have a clear separation of the support of the initial data and the ergoregion on  $\Sigma_0$ .

### 6.3. Grid size and parameters

The radial extent of the computational domain used in our simulations was chosen to be the closed interval  $-64 \leq r_* \leq 64$  in the massive case ( $M = 1$ ), whereas the closed interval  $0 \leq r_* \leq 64$  in case of the Minkowski limit ( $M = 0$ ). The specific angular momentum parameter  $a$  of the Kerr background was always chosen to be 0.9 while the Schwarzschild limit was achieved by taking  $a = 0$ . The evolution of the system was investigated in the time interval  $0 \leq t \leq 192$ . The fine tuned parameters of the initial data (6.4)—tuned to have the largest possible effect in superradiance—were  $\omega_0 = 0.313394503136629$ ,  $r_{*0} = 31.8229346475152$ ,  $w = 35.3679317843828$ , while the angular and azimuthal mode numbers  $\ell$  and  $m$  were fixed by choosing  $\ell = 2$  and  $m = -2, 0, 2$ . Accordingly, the initial data had pure quadrupole character, while for  $m$  the values  $-2, 0$  and  $2$  signifies counter-rotating, non-rotating and co-rotating initial distributions, respectively. In virtue of the above discussion we may only expect the appearance of superradiance in the co-rotating case with  $m = 2$ , while no or negligible effect may be anticipated in the non-rotating or counter-rotating cases with  $m = 0$  or  $m = -2$ , respectively.

In order to justify the above very specific choice made for the parameters  $\omega_0$ ,  $r_{*0}$  and  $w$  let us recall the list of requirements they have to satisfy.

- $(w/4)^{-1} \ll m\Omega_H \iff$  The width of frequency profile should be much smaller than the width of the superradiant frequency domain.
- $w \ll r_{*,\max} - r_{*,\text{ergosphere}} \iff$  The width of the initial data has to be much smaller than the part of the domain of outer communication outside to the ergosphere and covered by the grid.
- $w \gg \Delta r_* \iff$  The width and ramp of the wave packet has to be much larger than the spatial resolution of the base grid applied in AMR.
- $\omega_0 \ll \Delta t^{-1} \iff$  The leading frequency of the initial data has to be much smaller than the maximal frequency allowed by the temporal resolution of the base grid.
- $r_{*0} - \frac{1}{2}w > r_{*,\text{ergosphere}} \iff$  The support of the initial data has to be well separated from the ergoregion.
- $r_{*0} + \frac{1}{2}w < r_{*,\max} \iff$  The support of the initial data has to be included with suitable margins by the radial computational domain.

### 6.4. Generic initial data for GridRipper

Let us finally mention that in spite of the fact that in the investigations reported in this paper the initial data is always of pure multipole type in our code GridRipper (that can be downloaded from [20]) the generic case—whenever a multipole expansion of the initial data is required—is also implemented (see, e.g., [19] for an application). In the current



version of GridRipper this is done by simply integrating numerically the product of the basic variables with  $\bar{Y}_\ell^m$  over the  $r_* = \text{const}$  angular spheres on  $\Sigma_0$ . In order to make this part computationally inexpensive—reducing thereby the required computational time to the order of seconds—the very efficient and precise two dimensional adaptive Genz-Malik (AGM) method [47] is applied.

## 7. Numerical investigations

This Section is to introduce our main results concerning the evolution of a massless scalar field on Kerr background. As emphasized earlier distinguished attention will be paid to the angular dependence of the field and to the formation of superradiance. Before presenting our numerical results it is important to justify the reliability of the proposed new method.

### 7.1. Error estimates and convergence

As emphasized in Section 3 the representation of the basic variables by truncated multipole series can only be ‘exact’ in the case of linear field equations. On the other hand, whenever the evolution equations contain non-linear expressions of the basic variables—with non-trivial angular dependencies—the multipole method becomes inherently perturbative. Nevertheless, it is believed that the error yielded by the truncation of the infinite multipole series remains at a tolerable level provided that the value of  $\ell_{\max}$  is kept at a sufficiently high value. In order to demonstrate that this expectation is valid, the  $\ell_{\max}$  dependence of some estimates on the error and the convergence will be shown below.

Almost all of our simulations were performed by using  $\ell_{\max} = 12$ , nevertheless, in order to be able to determine the convergence rate simulations with  $\ell_{\max} = 14, 16$  and  $18$  were also performed in the Kerr case with initially co-rotating and counter rotating distributions. Note that as the initial data had pure quadrupole character the indicated variation of the value  $\ell_{\max}$  had no effect on it.

In what follows the numerical representation—with maximal multipole order  $\ell_{\max}$ —of a function  $f$  will be denoted by  $f_{\ell_{\max}}$ . Assume that  $\Delta\ell_{\max}$  is some positive integer. As a measure of the relative error of the variable  $f_{\ell_{\max}}$  the quantity

$$E_{\ell_{\max}, \Delta\ell_{\max}}(f) = \frac{\|f_{\ell_{\max}} - f_{\ell_{\max} + \Delta\ell_{\max}}\|}{\|f_{\ell_{\max} + \Delta\ell_{\max}}\|} \quad (7.1)$$

was applied. Notice that  $E_{\ell_{\max}, \Delta\ell_{\max}}(f)$  monitors the time dependence of the difference of the basic and finer solutions  $f_{\ell_{\max}}$  and  $f_{\ell_{\max} + \Delta\ell_{\max}}$  relative to the finer one. The norm  $\|\cdot\|$  applied here, and in (7.2) below, is the  $C^0$  norm bounded from above by the second Sobolev norm  $C\|\cdot\|_{H_2^2(\mathbb{S}^2, \mathbb{C})}$ , where  $C$  is the minimal Sobolev constant associated with the  $H_2^2(\mathbb{S}^2, \mathbb{C}) \subset C^0(\mathbb{S}^2, \mathbb{C})$  Sobolev embedding as discussed in Appendix A and Appendix D. Clearly,  $E_{\ell_{\max}, \Delta\ell_{\max}}(f) \ll 1$  has to hold for reasonable numerical solutions provided that the value of  $\ell_{\max}$  is sufficiently large.

Another useful quantity characterizing the validity of the applied numerical schema is the d'Alembert convergence factor defined for the numerical representation  $f_{\ell_{\max}}$  as

$$Q_{\ell_{\max}, \Delta\ell_{\max}}(f) = \frac{\|f_{\ell_{\max} + \Delta\ell_{\max}} - f_{\ell_{\max} + 2\Delta\ell_{\max}}\|}{\|f_{\ell_{\max}} - f_{\ell_{\max} + \Delta\ell_{\max}}\|}. \quad (7.2)$$

This quantity measures the local convergence rate centered at  $\ell_{\max} + \Delta\ell_{\max}$ . In virtue of d'Alembert's criterion guaranteeing a sequence to be summable, convergence of the numerical solution in  $\ell_{\max}$  occurs provided that the inequality  $\limsup_{\ell_{\max} \rightarrow \infty} (Q_{\ell_{\max}, \Delta\ell_{\max}}(f)) < 1$  holds.

A related quantity—which is useful in quantifying the appropriateness of the numerical scheme—is the local exponent of convergence defined by the ratio

$$\frac{\ln(Q_{\ell_{\max}, \Delta\ell_{\max}}(f))}{\Delta\ell_{\max}}. \quad (7.3)$$

As discussed in Appendix E, whenever a function  $f$  is  $C^\infty$  the convergence has to be faster than any polynomial in  $\ell_{\max}$ , and therefore the local exponent of convergence becomes an informative measure of convergence rate—which is expected to be constant whenever the convergence is exponential.

On Figure 7.1 the time and  $\ell_{\max}$  dependencies of the relative error  $E_{\ell_{\max}, \Delta\ell_{\max}}(\Psi)$  relevant for the basic variable  $\Psi$  are shown for an initially co- or counter rotating massless scalar field on a Kerr background with parameters  $M = 1$  and  $a = 0.99$ . As it is clearly visible the relative error is always smaller than  $10^{-8}$  and it is decreasing while  $\ell_{\max}$  is increased. If considerations are restricted to the initial part of the evolution, i.e., to the part before the wave packets leave the computational domain at  $t \sim 75$ , the relative error does not exceed the level  $\sim 10^{-12}$ . Following this initial, truly dynamical, period eight order smaller amplitude quasi-normal ringing and finally an even smaller amplitude power low tail decay occur (see, e.g., [15]). The amplitude of these processes is comparable to the applied accuracy of the present simulations which yields a visible increase in the relative error. Notice also that the apparent linear hierarchy of the graphs—transparent in the applied logarithmic scale in both of the subregions—justifies that, indeed, the convergence rate in  $\ell_{\max}$  is exponential.

Let us mention here that as the finite differencing part of our code, applied in the “ $t - r$ ” Lorentzian sector, is exactly the one which, along with the AMR part, went through careful and detailed convergence tests—and the pertinent results can be found in [29, 30]—we would like to recall here only that this part of the code is of fourth order accurate as it should be according to the implemented numerical scheme.

The computational times as listed in Table 7.1—relevant for the same systems as described in connection with Figure 7.1 and also for the common PC architecture AMD Phenom(tm) 2.3GHz CPU—justify that the required computational resources are affordable, i.e. the proposed new method is computationally inexpensive.

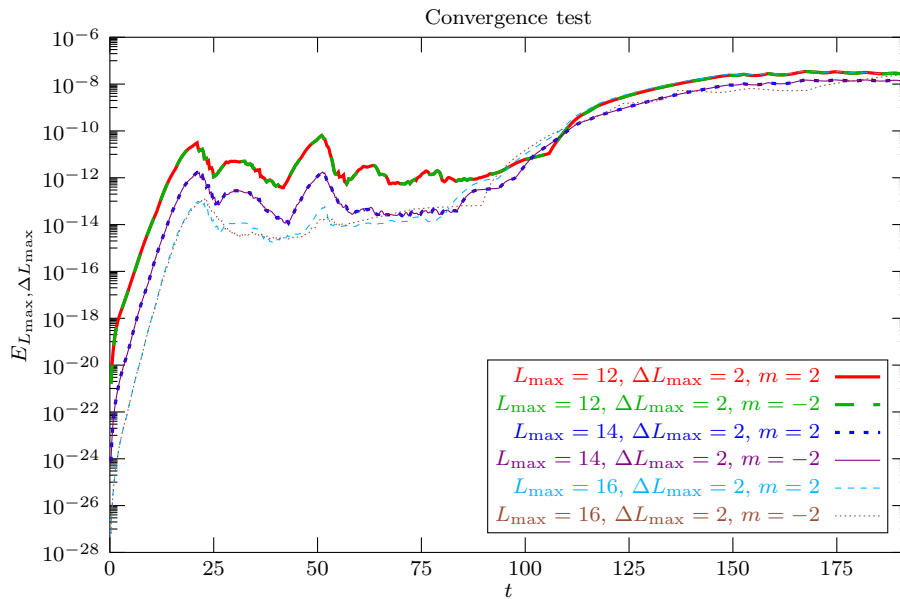


**Figure 7.1.** (Color online) The coordinate time and  $\ell_{\max}$  dependence of the relative error  $E_{\ell_{\max}, \Delta \ell_{\max}}(\Psi)$  of  $\Psi$  representing the evolution of initially co- or counter rotating massless scalar field with  $\ell = 2, m = 2$  or  $\ell = 2, m = -2$ , respectively, on a Kerr background with parameters  $M = 1, a = 0.99$  and for the particular values  $\ell_{\max} = 12, 14$  and  $16$  are shown. The apparent linear shifting of the error curves on this figure verify that the rate of convergence in  $\ell_{\max}$  is exponential.

$\ell_{\max}$	Comp. time ( $m = -2$ )	Comp. time ( $m = 2$ )
12	39582 sec	56374 sec
14	53274 sec	76089 sec
16	68900 sec	99248 sec
18	87514 sec	124727 sec

**Table 7.1.** The computation time of the evolution of initially co- or counter rotating massless scalar field with  $\ell = 2, m = 2$  or  $\ell = 2, m = -2$ , respectively, on a Kerr background with parameters  $M = 1, a = 0.99$  within the coordinate time interval  $0 \leq t \leq 192$  and with the particular choices of the values  $\ell_{\max} = 12, 14, 16$  and  $18$ . The indicated times were measured by using PCs with architecture AMD Phenom(tm) 2.3GHz CPU which justify that the proposed new method is computationally inexpensive.

## 7.2. Energy and angular momentum balances

In addition to the rate of convergence in  $\ell_{\max}$  the use of the energy and angular momentum balance relations provides another important consistency check verifying the reliability of the proposed numerical algorithm.

Recall that the balance laws relate values of energy and angular momentum on portions of  $t = \text{const}$  hypersurfaces to energy and angular momentum fluxes across the timelike hypersurfaces connecting the edges of them. In particular, the argument goes

as follows. Whenever there is a divergence free vector field  $J^a$  on a spacetime it can be justified by referring to Stokes' theorem that for a spacetime domain  $N$  with boundary  $\partial N$  and outward pointing unit normal vector  $n_a$  at  $\partial N$  the balance relation

$$\int_{\partial N} n_a J^a = \int_{intN} \nabla_a J^a = 0 \quad (7.4)$$

holds. On the other hand, it is well-known that—as the vector fields  $\partial_t$  and  $\partial_\varphi$  are Killing vectors on a Kerr spacetime—the contractions  $J_E^a = -T^a_b \partial_t^b$  and  $J_L^a = T^a_b \partial_\varphi^b$ , which are the energy and angular momentum currents, are divergence free, where  $T_{ab}$  denotes the energy-momentum tensor of the matter fields. In our investigations,  $N(t)$  was chosen to possess—in the tortoise Boyer-Lindquist coordinates—the form of the Cartesian product  $[0, t] \times [r_{*1}, r_{*2}] \times [0, \pi] \times [0, 2\pi]$ .

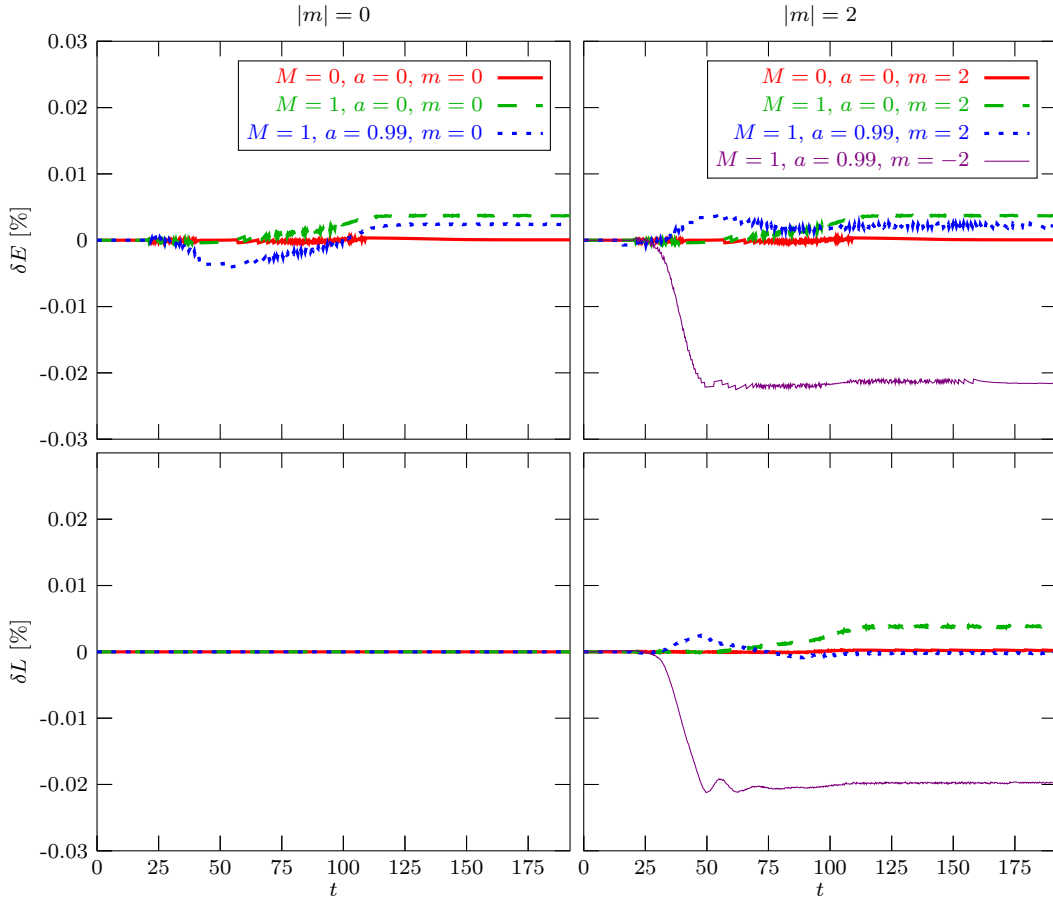


**Figure 7.2.** (Color online) The time dependence of the relative variation  $\delta E = \frac{1}{E_0} \int_{\partial N(t)} n_a J_P^a$  and  $\delta L = \frac{1}{L_0} \int_{\partial N(t)} n_a J_L^a$  of energy and angular momentum balances during the evolution of a massless scalar field on Minkowski, Schwarzschild and Kerr background spacetimes with initially co-rotating ( $m = 2$ ), non-rotating ( $m = 0$ ) and counter-rotating ( $m = -2$ ) pure quadrupole type initial data. The reference values  $E_0$  and  $L_0$  are the initial energy and angular momentum contents of the selected parts of the initial data surface  $t = 0$ , respectively.

The constant  $r_*$  values determining the edges of spatial section of the cylindrical

domain of integration  $N(t)$ —in order to keep some margin from the edges of the computational domain—were chosen to be such that  $r_{*1} = -63$  and  $r_{*2} = 63$  for the Kerr or Schwarzschild cases with  $M = 1$ , whereas  $r_{*1} = 0$  and  $r_{*2} = 63$  were used in the Minkowski limit with  $M = 0$ , where  $r_*$  reduces to  $r$ .

On Figure 7.2 the time dependence of the relative variation  $\delta E$  and  $\delta L$  of energy and angular momentum balance relations are shown. Here  $\delta E$  and  $\delta L$  are defined as

$$\delta E = \frac{1}{E_0} \int_{\partial N} n_a J_E^a \quad \text{and} \quad \delta L = \frac{1}{L_0} \int_{\partial N} n_a J_L^a, \quad (7.5)$$

where  $E_0$  and  $L_0$  denote the energy and angular momentum of the initial configuration within the spatial region  $r_* \in [r_{*1}, r_{*2}]$ . The graphs on Figure 7.2 make it transparent that the energy and angular momentum balances hold up to a remarkable precision for the entire evolution.

Note, finally, that the evaluation of the involved integrals can be done in a straightforward way in context of the spectral method as the integration with respect to the angular degrees of freedom can simply be given as  $L^2$  scalar products of the basic variables which can be evaluated as outlined in Appendices A, B, C and D. In addition, the integrals with respect to the radial and temporal directions were evaluated by using a fifth order integration scheme to avoid the loss of accuracy of the numerical data yielded by the applied fourth order finite difference scheme in the  $t - r_*$  plane.

### 7.3. Angular dependencies of the fields

After presenting the consistency checks of the applied numerical scheme let us turn to the description of the physical properties of the solutions. In this Section our main concern is the angular dependence of the evolving scalar field.

To have some hints regarding the dynamics of a massless scalar field with co-rotating quadrupole type data on Kerr spacetime the energy density and the momentum current distributions are shown on Figure 7.3 on the initial data surface, at  $t = 0$ , and on an intermediate time level surface after a scattering of the inward falling radiation has happened, at  $t = 48$ . It is visible that, in spite of the fact that the initial data was also fine tuned to be maximally superradiant, the dominant part of the outgoing radiation leaves the central region without indicating the slightest preference of directions close to the axis of rotation.

On Figure 7.4 the time dependence of both the total integrated fluxes of the radiated energy and angular momentum through the  $r_* = 63$  sphere and the fluxes of the radiated energy and angular momentum integrated on the caps of sphere yielded by the intersection of a double right circular rotationally symmetric cone with apex angle  $2\theta = \pi/3$  and the  $r_* = 63$  sphere is shown for various configurations.

It can be seen that in the case of rotating initial configuration (with  $m \neq 0$ ) the outgoing radiation is suppressed in the vicinity of the axis of rotation. An effective evaluation of the flux integrals on the caps of the sphere yielded by the intersection of

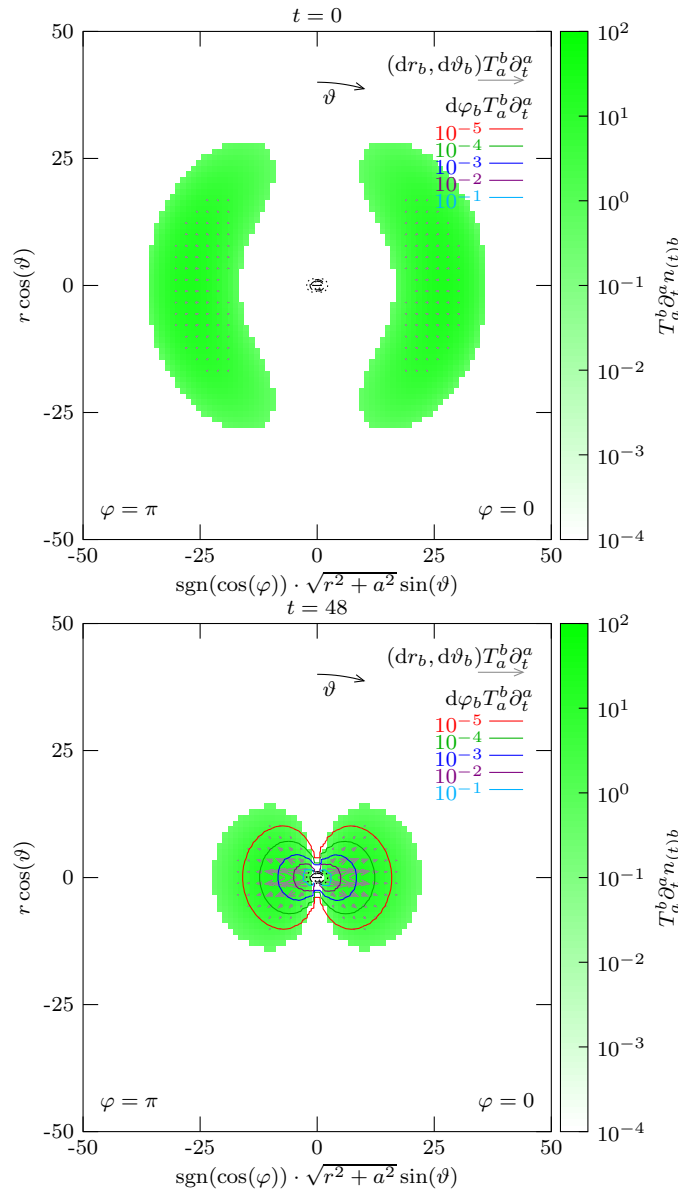


**Figure 7.3.** (Color online) The spatial distribution of energy density  $n_{(t)b} T_a^b \partial_t^a$  and the  $r, \vartheta, \varphi$  components of the energy current  $T_a^b \partial_t^a$  are shown at  $t = 0$  (top panel) and at  $t = 48$  (bottom panel) for a massless initially co-rotating scalar field on a Kerr background with parameters  $M = 1$  and  $a = 0.99$ . Note that only the sections corresponding to the azimuthal slices  $\varphi = 0$  and  $\pi$  are plotted. The initial data was fine tuned to be maximally superradiant and by  $t = 48$  a scattering has already happened. The energy density,  $n_{(t)b} T_a^b \partial_t^a$ , is indicated by the color map while the  $dr_b T_a^b \partial_t^a$  and  $d\vartheta_b T_a^b \partial_t^a$  components of the energy current tangent to the  $\varphi = 0$  and  $\pi$  plane are indicated by arrows, whereas the azimuthal component  $d\varphi_b T_a^b \partial_t^a$  is depicted by isocurves. The location of the singularity, the event horizon and the ergosphere is also indicated on central parts of the plots. Note that for the sake of simplicity the quantities indicated are given by referring to the Boyer-Lindquist coordinates.

a double right circular rotationally symmetric cone in the spectral framework requires

additional technicalities which are described in details in Appendix F.

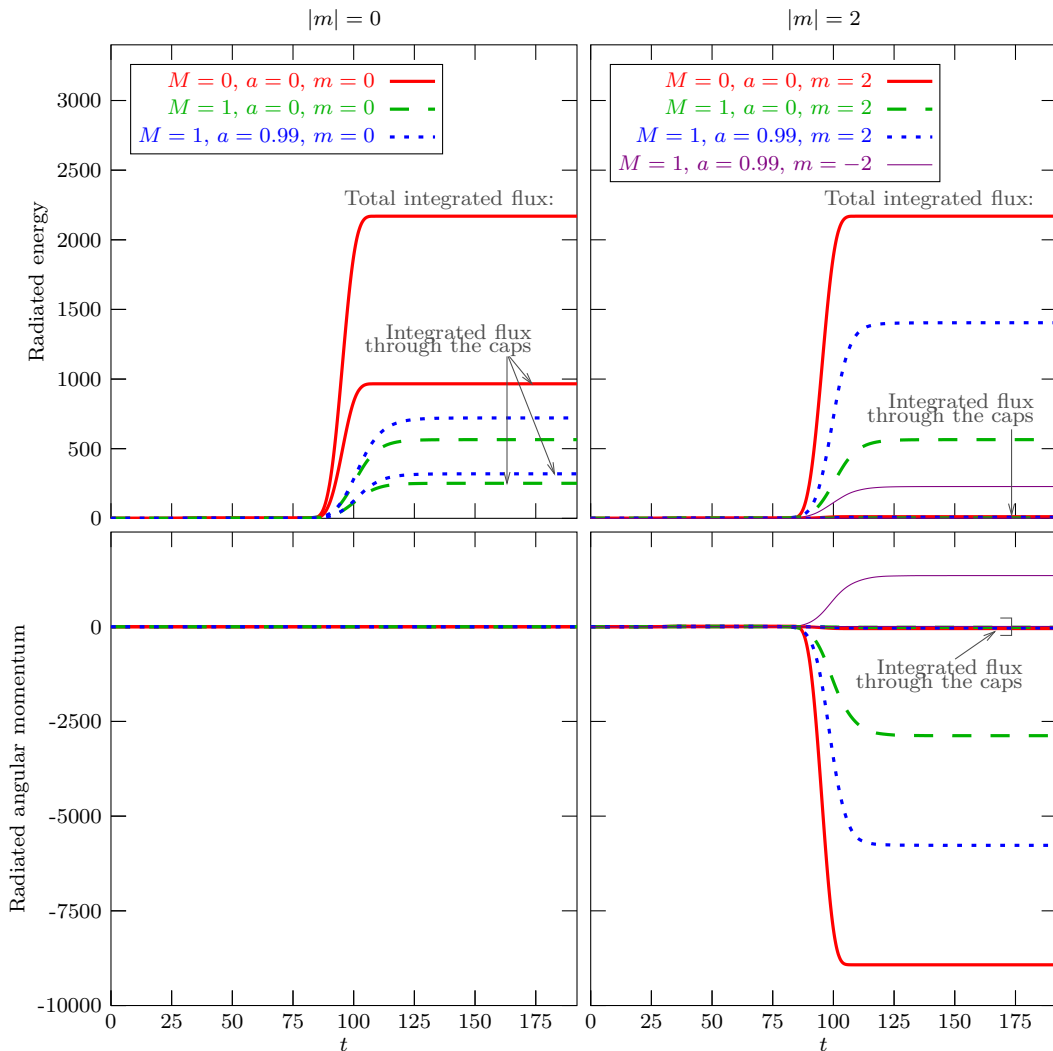


**Figure 7.4.** (Color online) The time dependence of the integrated energy and angular momentum fluxes during the evolution of an initially quadrupole type co-rotating ( $m = 2$ ), non-rotating ( $m = 0$ ) and counter rotating ( $m = -2$ ) massless scalar field on Minkowski, Schwarzschild and Kerr spacetimes is shown. Besides the total integrated fluxes the fluxes integrated on the disjoint caps of the sphere with radius  $r_* = 63$  yielded by the intersection of a double right circular rotationally symmetric cone with apex angle  $2\theta = \pi/3$  and the sphere are plotted. Note that in the Kerr case the co-rotating initial data with  $m = 2$  was fine tuned to be maximally superradiant.

It still remains really cumbersome to extract some insight concerning the anisotropy of the outgoing radiation simply by inspecting plots of the type depicted by Figs. 7.3 and 7.4. Therefore it is important to have a clear measure of anisotropy. Assume that  $J^a$  is a conserved current and consider a ball  $\mathcal{B}(\bar{r}_*)$  of radius  $r_* = \bar{r}_*$  in the outer region of the computational domain. Denote by  $\mathcal{B}(\bar{r}_*, \theta)$  the disjoint union of the two caps yielded by the intersection of a double right circular rotationally symmetric cone with apex angle  $2\theta$  and the ball  $\mathcal{B}(\bar{r}_*)$ . Clearly then  $\mathcal{B}(\bar{r}_*) = \mathcal{B}(\bar{r}_*, \pi/2)$ . Finally, denote

by  $X_{\text{out}}^J|_{\theta}(t)$  the integral  $\int_{[0,t] \times \mathcal{B}(\bar{r}_*,\theta)} n_{r_*a} J^a$ , where  $n_{r_*a}$  stands for the unit form field normal to the hypersurface  $[0, t] \times \mathcal{B}(\bar{r}_*, \theta)$ , i.e.  $n_{r_*a}$  points to the increasing  $r_*$  direction.

Based on the above introduced quantities, as a measure of anisotropy, we may use then the expression

$$\mathcal{A}^J(t, \theta) = \frac{\frac{1}{4\pi(1-\cos\theta)}}{\frac{1}{4\pi}} \frac{X_{\text{out}}^J|_{\theta}(t)}{X_{\text{out}}^J|_{\pi/2}(t_{\text{max}})} \quad (7.6)$$

which is nothing else but the ration of the time dependent angle average of the integrated flux of the current  $J^a$  through the two caps,  $\mathcal{B}(\bar{r}_*, \theta)$ , of the ball  $\mathcal{B}(\bar{r}_*)$  of radius  $r_* = \bar{r}_*$  located at the north and south poles and of the angle average of the total integrated flux through the entire ball  $\mathcal{B}(\bar{r}_*)$ .

Notice that, for any fixed  $\theta \in (0, \pi/2)$  value, whenever the radiation has no anisotropy at all  $\mathcal{A}^J(t, \theta)$  tends to 1 as  $t \rightarrow t_{\text{max}}$ , it tends to a value smaller than 1 if the radiation shows preferences of the directions close to the equatorial plane, while  $\mathcal{A}^J(t, \theta)$  tends to a value greater than 1 if the radiation prefers the axial directions. Clearly by choosing  $\theta$  to be small the sharp preference of the axis can be tested, whereas by increasing its value the anisotropy can be tested for a wider range of directions around the axis. In all of our investigation  $\theta$  was chosen to be  $\pi/6$ , i.e. all directions within a right circular rotationally symmetric cone with apex angle  $2\theta = \pi/3$  were included.

On Figure 7.5 the time dependence of the energy and angular momentum radiation anisotropies,  $\mathcal{A}^{J_E}(t, \pi/6)$  and  $\mathcal{A}^{J_L}(t, \pi/6)$  is shown for Kerr, Schwarzschild and Minkowski background spacetimes. The evolution starts with co-rotating or counter rotating initially field configurations. As before the co-rotating initial data was fine tuned to be maximally superradiant. By the inspection of Figure 7.5 the following simple observation can be made.

- Regardless whether the initial configuration was co-rotating or counter rotating a strong preference of the directions close to the equatorial plane is justified by the asymptotic behavior of  $\mathcal{A}^{J_E}(t, \pi/6)$  and  $\mathcal{A}^{J_L}(t, \pi/6)$  both of which tend to a value much smaller then 1.
- It is also clearly visible that the properties of the background spacetimes have no noticeable effect on the evolution of either  $\mathcal{A}^{J_E}(t, \pi/6)$  or  $\mathcal{A}^{J_L}(t, \pi/6)$ .
- Finally, the fact that the initial data for the co-rotating configuration was fine tuned to have the solution to be superradiant has no effect at all on the anisotropy of the energy and angular momentum distribution of the outgoing radiation.

#### 7.4. Superradiance and nearly perfect reflection

Based on the observed insensitivity of the anisotropy on the superradiant or non-superradiant character of the initial configuration it turned to be important to understand the reflection and absorption processes during the evolution of the investigated scalar field on black hole backgrounds.



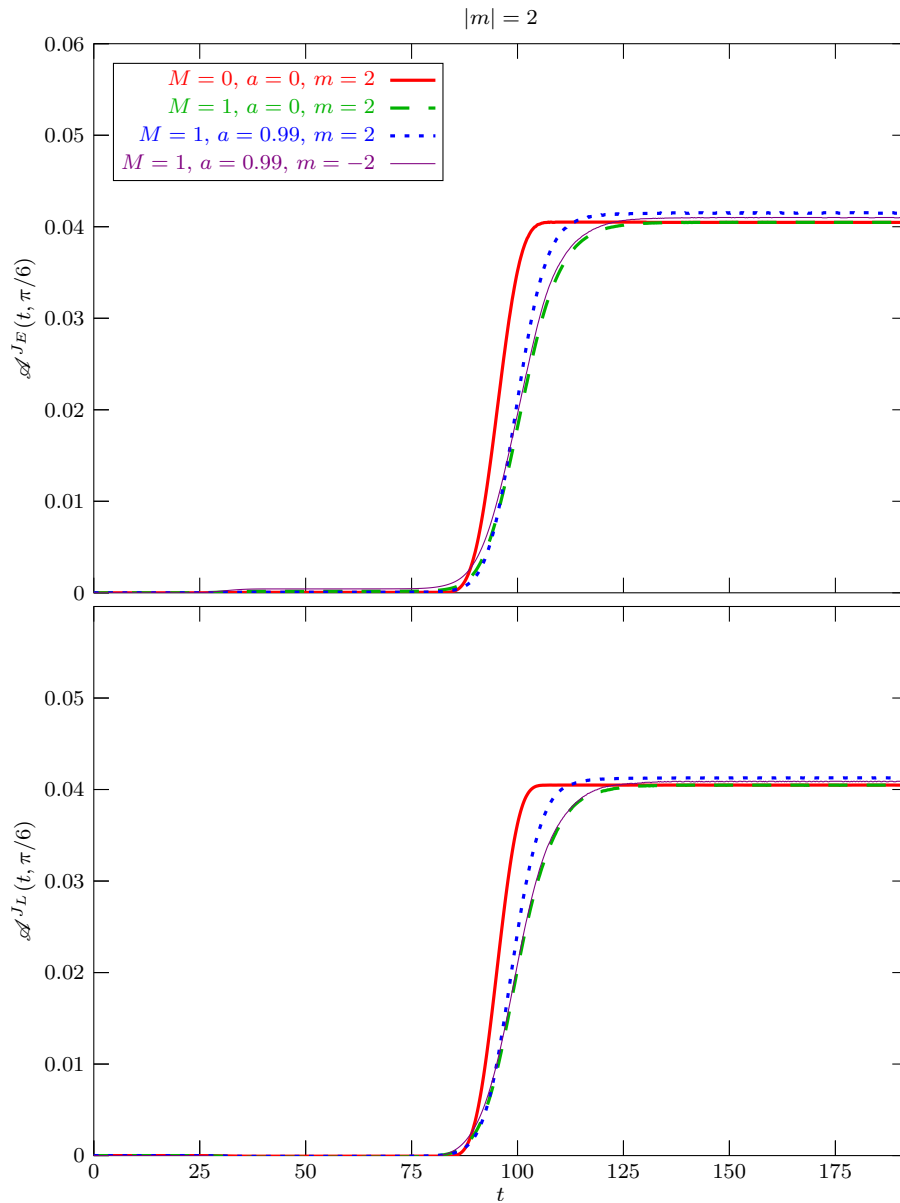


**Figure 7.5.** (Color online) The time dependence of the energy and angular momentum radiation anisotropies,  $\mathcal{A}^{J_E}(t, \pi/6)$  and  $\mathcal{A}^{J_L}(t, \pi/6)$ , is shown for Kerr, with  $M = 1$ ,  $a = 0.99$ , Schwarzschild, with  $M = 1$ ,  $a = 0$ , and Minkowski, with  $M = 0$ ,  $a = 0$ , backgrounds. The evolution starts with co-rotating or counter rotating initial field configurations. The co-rotating initial data was fine tuned to be maximally superradiant in the Kerr case.

As it was already indicated in subsection 6.2 it is important to be sure that the type of initial data chosen there does correspond to be superradiant configurations. To justify that this is indeed the case we determined the temporal frequency spectrum of a numerical solution with initial data parameters  $\omega_0 = \frac{1}{2}m\Omega_H$ ,  $r_{*0} = 31.823$ ,  $\ell = 2$ ,  $m = 2$  and with Kerr background parameters  $M = 1$ ,  $a = 0.99$  at the location  $r_* = 14$  which is located towards the black hole with respect to the compact support of the initial data.

It is clearly justified by Figure 7.6 that the spectrum is indeed well contained within the superradiant regime as expected.

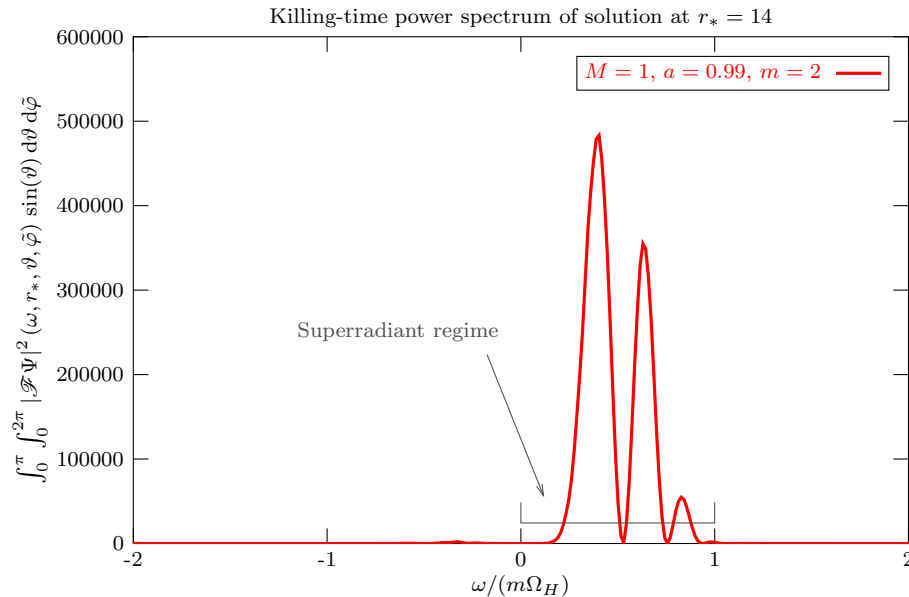


**Figure 7.6.** (Color online) The power spectrum in temporal frequency, at the location  $r_* = 14$ , of an inward traveling wave packet with  $\ell = 2$ ,  $m = 2$  and with initial data having leading frequency  $\omega_0 = \frac{1}{2}m\Omega_H$ . Thereby, the incident wave packet is, as it is expected, to be maximally superradiant. The parameters of the Kerr background were  $M = 1$ ,  $a = 0.99$ . Note that the spectrum appears to be relatively intact in its superradiant character, i.e. the solution remains in the desired frequency regime.

The generic behavior of the incident wave packets is depicted on Figure 7.7. This figure shows the time dependence of the radial coordinate densities of the energy and angular distributions of the massless scalar field evolving on Minkowski, Schwarzschild and Kerr background spacetimes. The initial data is of quadrupole type and co-rotating or counter rotating in the Kerr case, according to the choices  $\ell = 2$  and  $m = \pm 2$ .

The radial coordinate density of energy and angular momentum are the quantities  $\mathcal{E}$  and  $\mathcal{L}$  with the help of which the energy and angular momentum,  $E$  and  $L$ , on a  $t = \text{const}$  time level surface can be given as  $E = \int_{t=\text{const}} \mathcal{E} dr_*$  and  $L = \int_{t=\text{const}} \mathcal{L} dr_*$ , i.e. in  $\mathcal{E}$  and  $\mathcal{L}$  the energy and angular momentum densities are integrated with respect to the angular degrees of freedom, and they also involve the not yet integrated part of the 3-volume form induced on the  $t = \text{const}$  time level surfaces.

We have found that in case of a massive background with  $M > 0$  for non-superradiant type of initial configurations, as it is expected, considerable part of the incident wave packet gets to be absorbed by the black hole. However, for initial data fine tuned to generate a totally superradiant configuration—contrary to the generic expectations—no energy extraction from the black hole was observed. Instead a nearly total reflection of the wave packet occurs, as it is shown on the bottom right panel of Figure 7.7. Notice the similarities characterizing the evolution of the to be superradiant

initial data in the Kerr case (lower right panel) and the evolution of the scalar field on simple Minkowski background (top left panel) with no black hole in the setup.

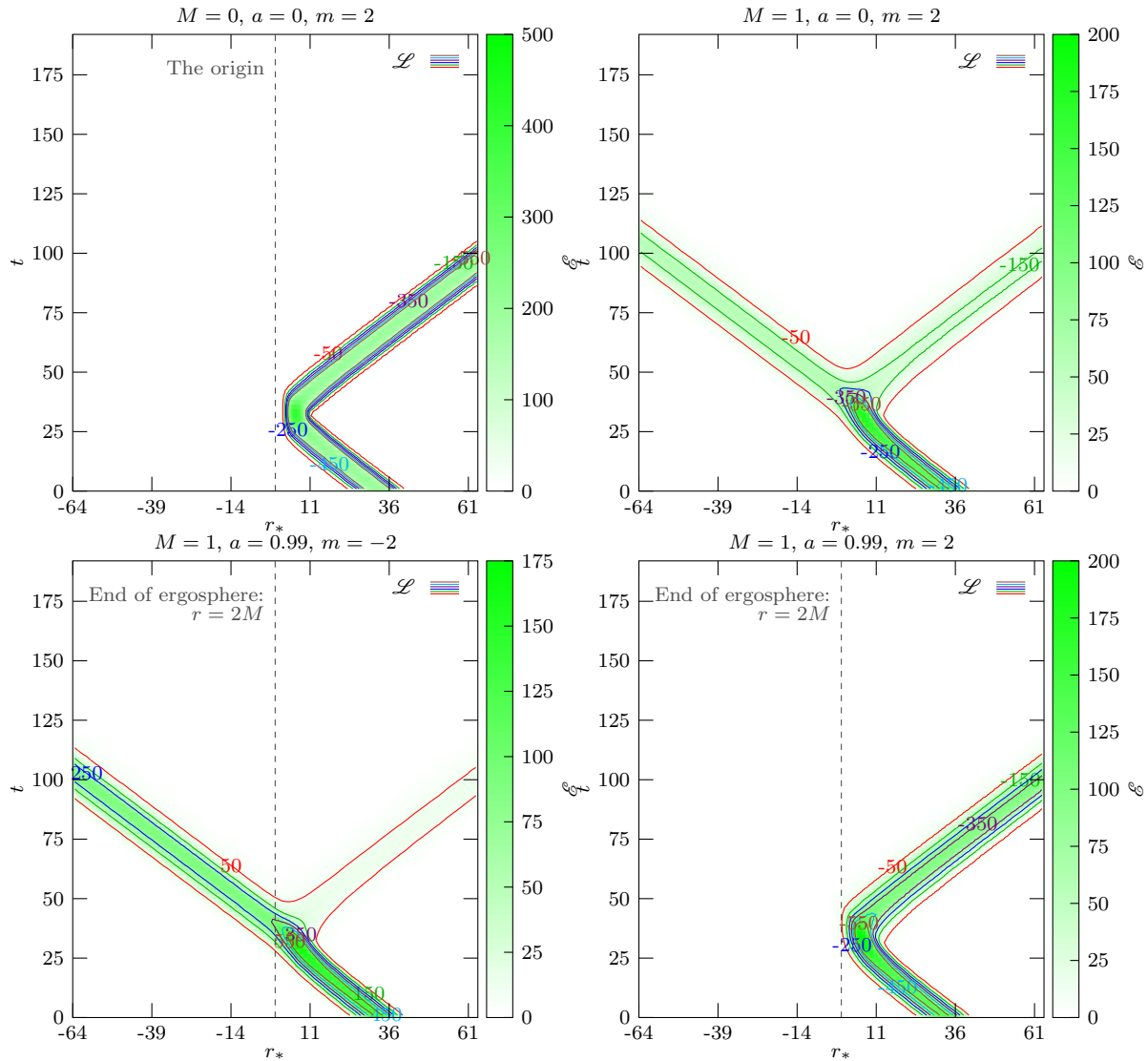


**Figure 7.7.** (Color online) The time dependence of the radial coordinate density of energy and angular momentum,  $\ell$  and  $\mathcal{L}$  (for their definition see the main text), is shown for Minkowski, Schwarzschild and Kerr background spacetimes. The evolution starts with co-rotating or counter rotating initially field configurations. As before the co-rotating initial data was fine tuned to be maximally superradiant in the Kerr case.

In trying to figure out the significance of this nearly perfect reflection recall now that to be able to produce extra energy in the process of superradiance substantial part of the radiation—after submerging into the ergoregion—has to descent towards the event horizon. The lack of energy extraction from the black hole can now be understood as the reflection happened before the radiation could have reached the ergoregion.

As our result concerning superradiance is on contrary to the conventional expectations it is important to emphasize that the observed phenomenon of this nearly

perfect reflection, for the part of the wave packet belonging to the superradiant regime, was found to be robust with respect to the variation of the parameters of the background spacetime and that of the initial data. Note also that as our pertinent results appear to be inconsistent with the claims [41, 42] it is important to clear up the reason beyond these controversial conclusions. In doing so start by recalling that there is a significant difference between the type of initial data applied in [41, 42] and in this paper. While the initial configuration we applied is of compact support in [41, 42] the initial data was arranged to have non-trivial values everywhere in the ergoregion. Moreover, it is claimed in [41, 42] that energy extraction from the black hole does occur. However, in our checks—applying horizon penetrating slices as in [15] and exactly the same type of initial data as in [41, 42]—the to be superradiant character of the field was lost in an extremely short period, more importantly, no energy flux leaving the ergoregion could be observed. All of these observations should be completed by emphasizing that our conclusions are not at all incompatible with claims in [43, 44, 45]. First of all, although in [44] compactly supported data is applied in deriving analytic estimates concerning superradiance the yielded results therein are converted, on page 833, to quantitative estimates based on approximations derived by Starobinskii [43], in spite of the fact that the approximations applied in [43] are not entirely compatible with the use of compactly supported initial data. What is even more important is that the pertinent conclusion in [44] provides only an upper bound for the gained energy which is about  $\sim 1\%$  for the case  $\ell = m = 2$ . Note also that our numerical findings are consistent with the upper bound,  $0.05 - 0.08\%$  for  $\ell = 2$  modes, on the scale of the energy extraction which we deduced by making use of a detailed single mode analysis (the results of which will be published elsewhere).

In providing some more convincing evidences let us emphasize first that the conventional arguments of Misner and Zel'dovich supporting the existence of energy extraction are based on the use of individual modes. Note, however, that the study of the linear stability problem for Kerr spacetimes [45], with the application of finite energy wave packets, taught us the lesson that statements at the level of individual modes need not imply statements for the superposition of infinitely many modes.

Figure 7.8 is to provide an additional justification of our main result. On this figure the time dependence of the energy extraction coefficient,  $\frac{\mathcal{E}_0 - \mathcal{E}_{\text{out}}}{\mathcal{E}_0}$  is shown, where  $\mathcal{E}_0$  and  $\mathcal{E}_{\text{out}}$ , respectively, stand for the initial value of the energy and for the integrated energy flux through the ball of radius  $r_* = 63$  located at the outer boundary of the computational domain. As it is visible the graph of  $\frac{\mathcal{E}_0 - \mathcal{E}_{\text{out}}}{\mathcal{E}_0}$  starts at the value one and tend to zero from above. Note that the slowly decreasing part, with  $150 \leq t \leq 1000$ , represents only the beginning of a long lasting quasi-normal ringing of the scalar field on the black hole background. The energy stored in these ringing modes will eternally be also radiated to infinity (see, e.g., [15]). Since  $\frac{\mathcal{E}_0 - \mathcal{E}_{\text{out}}}{\mathcal{E}_0}$  does not change sign the energy radiated to infinity remain always smaller than  $\mathcal{E}_0$ , which justify our conclusion that no energy extraction had happened.

Clearly, one could claim that any numerical method has its own limitation which

is true also in the present case. Nevertheless, in virtue of Figure 7.2 the accuracy of our numerical scheme allows us to put sharp upper bound on energy extraction which is  $\sim 10^{-3} - 10^{-4}$  times  $\mathcal{E}_0$  that is significantly smaller than the  $\sim 1\%$  of  $\mathcal{E}_0$  derived by analyzing individual modes [21, 22, 43].

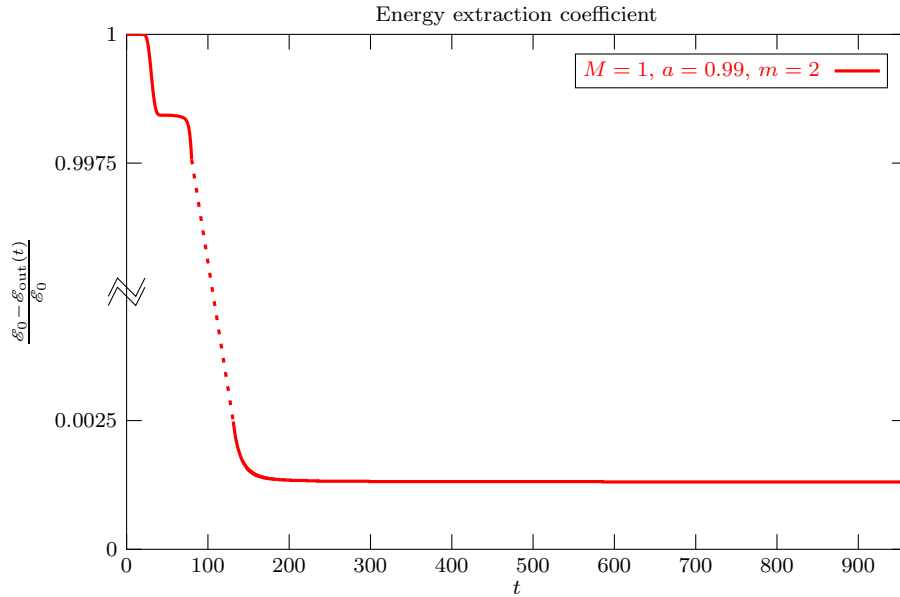


**Figure 7.8.** (Color online) The time dependence of the energy extraction coefficient,  $\frac{\mathcal{E}_0 - \mathcal{E}_{\text{out}}}{\mathcal{E}_0}$  is shown for quadrupole type initial data, where  $\mathcal{E}_0$  and  $\mathcal{E}_{\text{out}}$ , respectively, stand for the initial value and for the integrated energy flux through the sphere of radius  $r_* = 63$  located outward with respect to the support of the initial data.

Let us finally mention that the power spectrum in temporal frequency of the solution provides some new insight what happens whenever the to be superradiant wave packet approaches the ergosurface. On Figure 7.9 the  $r_*$  dependence of the power spectrum in temporal frequency of the solution, which had been averaged for the angular degrees of freedom, is shown. The initial data is exactly the same quadrupole type with  $\ell = m = 2$  as used to generate the solution depicted on Figure 7.7. (Note that to determine the proper Fourier transform of the solution for all the indicated values of  $r_*$  it was necessary to evolve the initial data both forward and backward in time.) It is clearly visible that the solution stays in the superradiant regime not only in the distant region but up to the ergoregion. In addition, it is also important that the frequency of the involved modes grows up to reaching the value  $\omega = m\Omega_H$  where, in virtue of the relation  $(\omega - m\Omega_H) |\mathcal{T}|^2 = (1 - |\mathcal{R}|^2)\omega$ , inevitably a total reflection has to occur.

Let us close this Section by commenting the non-negligible reflection visible on the top right panel of Figure 7.7 depicting the evolution of the massless scalar field on a Schwarzschild background. One might be surprised by this reflection as intuitively it is tempting to assume that the Schwarzschild black hole would be ready to absorb almost the entire of the incident wave packet. Recall, however, that the angular momentum

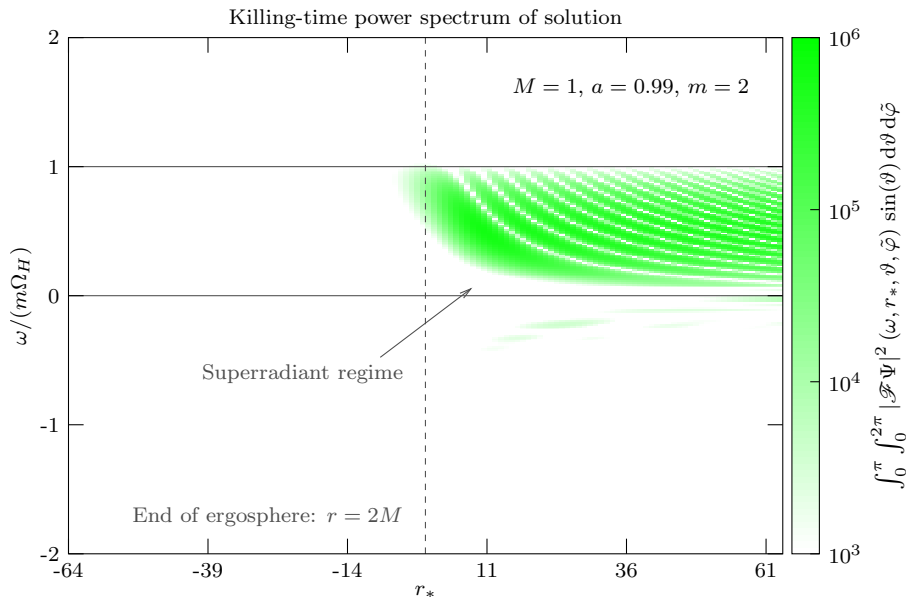


**Figure 7.9.** (Color online) The  $r_*$  dependence of the power spectrum in temporal frequency of the solution, which had been averaged for the angular degrees of freedom, is shown. The applied initial data is exactly the same quadrupole type with  $\ell = m = 2$  as used to generate the solution depicted on Figure 7.7. The solution stay in the superradiant regime for the entire evolution while the frequency of the involved modes grows up to reaching the value  $\omega = m\Omega_H$  where total reflection has to occur.

balance relation does not support the occurrence of such an overwhelming absorption. In addition it is also worth to have a look at the equation on a Schwarzschild background governing the evolution of a pure  $Y_\ell^m$  mode. In fact, the  $t - r_*$  part of the wave equation for the coefficient  $\Psi_\ell^m = \Psi_\ell^m(t, r_*)$  reads as

$$(\partial_t^2 - \partial_{r_*}^2) \Psi_\ell^m + V_\ell(r) \Psi_\ell^m = 0 \quad (7.7)$$

with the potential  $V_\ell(r) = (1 - \frac{2M}{r}) \left( \frac{\ell(\ell+1)}{r^2} + \frac{2M}{r^3} \right)$ . The repulsion—responsible for the reflection of the inward falling radiation and, in turn, leading to the celebrated power decay law of Price [48, 49]—is transparent on Figure 7.10 depicting the potential  $V_\ell(r)$  for the  $\ell = 0, 1, 2$  cases. What is really important here is that the maximum value of the potential  $V_{\ell=2}^{\max} \approx 0.24$  is significantly larger than  $\omega_0^2 \approx 0.096$  which, in virtue of the types of arguments contained e.g. by Section II of Chapter III in [46], can be used to justify the observed scale of reflection.

## 8. Summary

Our main concern in writing up this paper were at least two folded. On the one hand, we intended to introduce the generic setup of a method that is expected to provide a powerful new tool in studying the problem of time evolution of non-linear dynamical systems in four-dimensional spacetimes. On the other hand, we applied the introduced new method to study the evolution of a specific dynamical system. More precisely, the

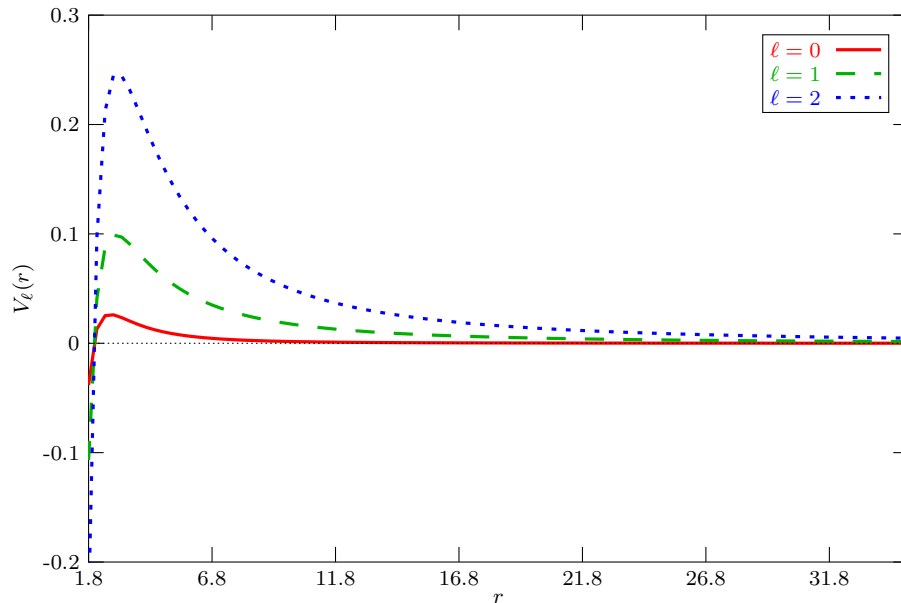


**Figure 7.10.** (Color online) The potential  $V_\ell(r)$  involved in the wave equation over Schwarzschild spacetime is plotted for values  $\ell = 0, 1, 2$ . The potentials have their common zero value at the horizon,  $r = 2M$ , while they attain their maximum close to but on the domain of outer communication side of the event horizon. The occurrence of the partial reflection on a Schwarzschild black hole background can be understood by taking into account the repulsing character of this potential, along with the fact that the maximum value of the potential  $V_{\ell=2}^{\max} \approx 0.24$  is significantly larger than  $\omega_0^2 \approx 0.096$ .

evolution of a massless scalar field on a fixed Kerr spacetime was investigated such that distinguished attention was paid to the angular distribution of the evolving field and to the occurrence of superradiance.

In spite of the fact that the mathematical background of the introduced new method—which is mainly contained by the appendices—makes it to be applicable to dynamical systems the time level surfaces of which can be foliated by a one-parameter family of codimension two surfaces which are conformal to a compact Riemannian manifold  $\mathcal{C}$  without boundary, in most of the cases with time level surfaces possessing the topology of  $\mathbb{R}^3$  or  $\mathbb{R} \times \mathbb{S}^2$  it suffices to assume that  $\mathcal{C}$  is topological two-sphere  $\mathbb{S}^2$ .

One of the main advantages of the new method is that it is fully spectral—not pseudospectral—in the angular directions. Thereby, whenever the basic variables are guaranteed to be at least of class  $C^2$  in the angular directions, the spectral components—even though non-linear expressions of the basic variables are involved—can be evolved without their steady pointwise evaluations. Accordingly, the angular degrees of freedom—directions tangential to  $\mathcal{C}$ —are treated by applying  $L^2$  expansions of the basic variables in terms of the eigenfunctions of the Laplace operator on  $\mathcal{C}$ . The corresponding expansion coefficients of a basic variable are evolved in the transverse 1+1 dimensional spacetime directions by making use of the method of lines based on a

fourth order finite difference numerical scheme such that the adaptive mesh refinement (AMR) is also incorporated.

The main advantages associated with the use of the proposed new method are:

- the coordinate singularities associated with the angular differential operators are treated in a fully analytic way
- all the non-linear operations such as multiplication of the basic variables or the division of an expression by a nowhere vanishing variable—the latter can be traced back to multiplication with the help of the Neumann series expansion—can be treated within the spectral representation without steady pointwise evaluation of these expressions
- a very effective treatment of an origin of the time level surfaces can also be done by making use of fully analytic considerations.

On some of the limitations of the proposed numerical method:

- The angular resolution, determined by the prefixed global value of  $\ell_{\max}$ , is not adaptive in the present implementation of our PDE solver. This may lead to the loss of accuracy in case of dynamical systems developing highly variable angular dependencies. This drawback, however, could be cured, if necessary, by endowing  $\ell_{\max}$  with a modest ‘ $t-r$ ’ dependence during the evolution, which could be controlled by a predefined tolerance in the measure of the tail sum error (see Appendix E for its detailed description).
- It should also be mentioned here that in case of dynamical systems with turbulent instabilities, i.e. for configurations which, at certain locations, require a simultaneous and substantial increase of both radial and angular resolutions, our method (such as many others) may turn to be highly suboptimal as even an adequate local splitting  $\mathbb{R}^2 \times \mathcal{C}$  may not be found to such a system.

A systematic self contained presentation of the mathematical background of the applied results and the implemented elements of the spectral method can be found in the appendices.

The introduced new numerical method is used to study the time evolution of a massless Klein-Gordon field on a fixed Kerr black hole spacetime. We would like to emphasize that this dynamical system is already complex enough to explore the main technical elements of the proposed numerical framework. In particular, two of the most important ones, i.e. the evaluation of various multilinear expressions and the division by a function based on the use of spectral method were applied in carrying out all of our simulations.

As all the multipole expansion series are truncated at certain finite order,  $\ell_{\max}$ , the proposed numerical method is perturbative. By studying the error introduced by the involved approximations it was verified that the error can be kept at a tolerable low level by applying sufficiently many members of the multipole expansions. In addition, a suitable notion of convergence was also introduced, based on d’Alembert’s criterion



guaranteeing the summability of sequences. It was justified that the convergence is exponential in the value of  $\ell_{\max}$ .

In studying the time evolution of a massless Klein-Gordon field on a fixed Kerr black hole distinguished attention was paid to the precise characterization of the angular dependence of the outgoing radiation, as well as, to the development of superradiance. Our main related results are as follows.

- There are attempts (see, e.g. [16, 17]) aiming to provide a simple and viable physical explanations of high energy collimated matter streams originating from compact astrophysical objects by applying Penrose process, or superradiance. On contrary to the underlying speculations we have found that the outgoing radiation has no preference at all of the axial directions regardless whether the initial configuration was to be superradiant or a more generic type.
- In studying superradiance—in the particular case of a massless scalar field—we intended to investigate its formation by using an incident wave packet, which was fine tuned to have the largest possible part of its frequency content within the superradiant regime, from the outer region of the domain of outer communication. On contrary to the general expectations, we found that instead of the expected scale of energy extraction from the black hole the incident wave packet failed to reach the ergoregion. Thereby, instead of superradiance, as an interesting phenomenon a nearly total reflection occurs before the “to be” superradiant part of the incident wave packet reaches the ergoregion. A complete characterization of this phenomenon definitely exceeds the scopes of the present paper. We plan to carry out its further investigations, involving possibly more generic type of initial data and, more importantly, a mixture of analytic and numerical techniques.

Concerning the required computational resources it is also important to be emphasized that various implementations of pseudospectral methods even in case of the study of time evolution of a massless Klein-Gordon field on a fixed Kerr black hole require powerful computers and parallel computing. As opposed to these the proposed new method was found to be very effective in the sense that time evolutions of the very same dynamical systems could be done within reasonable computational time on a stand-alone average personal computer without making use of parallel computing. We would also like to mention that the GPU implementation of the proposed method, which is under development, promises a further significant boost in the optimal use of the computational resources which will be inevitable in studying the evolution of more complicated non-linear dynamical systems.

Finally, we would like to emphasize that our code GridRipper, together with the implementation of the of time evolution of a massless Klein-Gordon field on a fixed Kerr background and other examples, is made available for public use and it can be downloaded from [20].

## Acknowledgments

We thank G. Z. Tóth for useful discussions and the organizers of the workshop(s) on “Quantitative Studies of Nonlinear Wave Phenomena” held at Ervin Schrödinger Institute—where parts of the reported results were developed—for their invitation and hospitality. The authors should also like to thank to projects maintaining the HunGrid VO of the LHC Computing Grid and a standalone cluster, both located at the computer center of Wigner RCP, for the access of their computational resources. This research was supported in part by OTKA grant K67942.

## Appendix A. Theory of Multipole Expansion of Multilinear Expressions

Let us start by recalling some of the basic notions and notations that we shall apply throughout the succeeding appendices. By a Riemannian manifold  $M$  we shall always mean an  $n$ -dimensional paracompact manifold (possibly with boundary) of differentiability class  $C^r$  endowed with Riemannian metric  $g$ , which will usually be suppressed. We shall denote by  $L^2(M, \mathbb{C})$  the Hilbert space of square-integrable complex valued functions<sup>¶</sup> on a Riemannian manifold  $M$ , and by  $C^l(M, \mathbb{C})$  the vector space of  $l$ -times continuously differentiable complex valued functions on  $M$ , where  $0 \leq l \leq r$ . Similarly,  $C_b^l(M, \mathbb{C})$  stands for the Banach space of bounded  $C^l(M, \mathbb{C})$  functions on  $M$  equipped with the  $C^l$  supremum norm, while  $C_\infty^l(M, \mathbb{C})$  denotes the Banach subspace of  $C_b^l(M, \mathbb{C})$  functions on  $M$  which have zero limit at infinity.<sup>+</sup>

Consider now the vector space of  $r$ -times weakly differentiable complex valued functions over  $M$ . The Sobolev norm of a function  $f$  belonging to this linear space is defined as

$$\|f\|_{H_r^2(M, \mathbb{C})} = \sqrt{\sum_{l=0}^r \int_M |\nabla^{(l)} f|^2}, \quad (\text{A.1})$$

where  $|\cdot|$  denotes the pointwise norm generated by the Riemann metric  $g$ ,  $\nabla$  denotes the Levi-Civita covariant derivation determined by  $g$ , while the associated volume form is suppressed in the applied notation. It is important to keep in mind that the highest,  $r^{\text{th}}$ -order, derivation in the above formula is required to be defined in the weak sense. The subset of the vector space of  $r$ -times weakly differentiable complex valued functions over  $M$  comprised by elements whose Sobolev norm  $\|\cdot\|_{H_r^2(M, \mathbb{C})}$  is finite is called the Sobolev space and it is denoted by  $H_r^2(M, \mathbb{C})$ . The Sobolev space together with its norm

<sup>¶</sup> Here in a precise formulation instead of ‘functions’ function equivalence classes should be used, where two Lebesgue measurable functions are considered to be equivalent if they are almost everywhere equal. Referring to these function equivalence classes as simply ‘functions’ is a common practice in functional analysis which we also shall use.

<sup>+</sup> A  $C_b^l(M, \mathbb{C})$  function is said to have zero limit at the infinity, if for any monotonously growing sequence of compact sets covering  $M$ , the  $C^l$  supremum norm of  $f$  over the complement of the compact sets tends to zero.

forms a Hilbert space, since its norm is generated by an inner product, and also it is complete with respect to this norm.

Let  $n$ ,  $r$  and  $k$  be non-negative integers, such that  $r > \frac{n}{2} + k$ . The classical result of Sobolev embedding theorem (see e.g. [50]) asserts then that the relation

$$H_r^2(\mathbb{R}^n, \mathbb{C}) \subset C_\infty^k(\mathbb{R}^n, \mathbb{C}) \quad (\text{A.2})$$

holds, and also that there exists a positive real constant  $C$  such that the inequality

$$\|\cdot\|_{C_\infty^k(\mathbb{R}^n, \mathbb{C})} \leq C \|\cdot\|_{H_r^2(\mathbb{R}^n, \mathbb{C})} \quad (\text{A.3})$$

is satisfied. These assertions are also known to hold [50] if  $\mathbb{R}^n$  is replaced by a compact subset in  $\mathbb{R}^n$ . In the next part of this appendix, our aim is to provide a simple and self-contained justification of the fact that the Sobolev embedding theorem may also be applied in case of compact Riemann manifolds.\* For yet another alternative reasoning see, e.g., Ref. [51].

In doing so consider first a finite dimensional real vector bundle,  $W(M)$ , of differentiability class  $C^r$  over a manifold  $M$  that belongs to the same differentiability class. Then, a pointwise mapping of  $C^r$ -sections of  $W(M)$  onto  $C^0$ -sections of  $M \times \mathbb{R}$  will be called to be a  $C^r$ -norm field if its pointwise restrictions to the fibers give rise to norms.† Indeed, every finite dimensional  $C^r$ -vector bundle over a paracompact manifold  $M$  admits  $C^r$ -norm fields. To see this recall that a norm field can always be defined locally over a coordinate chart, e.g., by taking in every point the natural Euclidean norm defined by a trivialization. These locally defined norm fields may, then, be sewn together by making use of a partition of unity subordinate to a locally finite collection of coordinate charts on  $M$ . The norm fields over a vector bundle are equivalent as it is justified by the following lemma.

**Lemma 1.** *If  $|\cdot|$  and  $|\cdot|'$  are  $C^r$  norm fields over  $W(M)$ , then there exists a positive real  $C^r$  field  $C$ , such that  $|\cdot|' \leq C|\cdot|$ .*

*Proof.* The proof is based on the paracompactness of  $M$  and on the equivalence of norms on a finite dimensional vector space.

To start of consider a locally finite atlas  $\mathcal{A} = \{(U_i, \varphi_i) \mid i \in I\}$  of  $M$  with partition of unity  $\{\mathcal{F}_i \mid i \in I\}$  such that each  $U_i$  has compact closure, denoted by  $\overline{U}_i$ , in  $M$ . Assume that the dimension of the fibers of  $W(M)$  is  $N$ . Let us fix a trivialization  $(e_{i,j} \mid j \in \{1, \dots, N\})$  of  $W(M)$  over each particular chart  $(U_i, \varphi_i) \in \mathcal{A}$ .

As a consequence of the equivalence of norms on a finite dimensional vector space, for any  $p \in M$  there exists a positive number  $c_p$ , such that  $|\cdot|'_p \leq c_p |\cdot|_p$ . Furthermore,

$$c_p \text{ may be chosen to be } \sup_{s_p \in W_p(M) \setminus \{0_p\}} \frac{|s_p|'_p}{|s_p|_p}.$$

\* Note, however, that there are non-compact Riemann manifolds such that the Sobolev embedding theorem does not apply to them.

† A more adequate way of formulating this definition is that a  $W(M) \rightarrow M \times \mathbb{R}$   $C^0$  fiber bundle homomorphism is a  $C^r$  norm field if its restrictions to the fibers are norms.

By making use of the trivialization  $(e_{i,j})$  of  $W(M)$  over  $(U_i, \varphi_i)$  it can be verified immediately that

$$\sup_{p \in \bar{U}_i} \left( \sup_{s_p \in W_p(M) \setminus \{0_p\}} \frac{|s_p|'_p}{|s_p|_p} \right) = \sup_{p \in \bar{U}_i} \left( \sup_{S \in \mathbb{R}^N, |S|=1} \frac{|\sum_{j=1}^N S_j e_{i,j}|'(p)}{|\sum_{j=1}^N S_j e_{i,j}|(p)} \right) \quad (\text{A.4})$$

holds for any choice of  $(U_i, \varphi_i) \in \mathcal{A}$ . The right hand side of (A.4) is a finite positive number, because it is nothing but the maximum of a positive valued continuous function over the compact manifold  $\bar{U}_i \times \mathbb{S}^{N-1}$ , where  $\mathbb{S}^{N-1}$  denotes the  $N - 1$  dimensional unit sphere. Let us denote this positive number by  $c_i$ . Then,

$$|\cdot|' \leq c_i |\cdot| \quad (\text{A.5})$$

holds over  $\bar{U}_i$ .

As an immediate consequence of (A.5) we have that  $\mathcal{F}_i |\cdot|' \leq c_i \mathcal{F}_i |\cdot|$  holds throughout  $M$ , in accordance with the fact that  $\mathcal{F}_i$  is non-negative and  $\text{supp}(\mathcal{F}_i) \subset U_i$ . Note, then, that the sum  $\sum_{i \in I} c_i \mathcal{F}_i$  is a positive valued  $C^r$  function—which, as a consequence of the local finiteness of  $\mathcal{A}$ , has only finite non-zero terms in a sufficiently small neighborhood of any point in  $M$ —, and that by definition  $\sum_{i \in I} \mathcal{F}_i = 1$ . These, along with the above observations, implies then that  $|\cdot|' \leq (\sum_{i \in I} c_i \mathcal{F}_i) |\cdot|$  holds, which justifies the assertion of the lemma.  $\square$

We shall also apply the following two lemmas in verifying that the Sobolev embedding theorem may also be applied in case of compact Riemann manifolds.

**Lemma 2.** *Let  $(|\cdot|_l)_{l \in \{0, \dots, m\}}$  be norm fields, and  $\nabla, \nabla'$  be two  $C^r$ -covariant derivative operators. Then, there exists a positive  $C^r$ -function  $C$  over  $M$  such that*

$$\sum_{l=0}^r |\nabla'^{(l)} \cdot|_l \leq C \sum_{l=0}^r |\nabla^{(l)} \cdot|_l. \quad (\text{A.6})$$

*Proof.* The assertion of this lemma may be justified by combining the following sequence of simple observations.

- (i) the covariant derivation  $\nabla'$  can always be expressed as a sum of terms involving  $\nabla$  and the  $C^{r-1}$  class Christoffel symbols,
- (ii) the triangle inequality holds for norms,
- (iii) the composition of a norm with a linear map is a semi-norm,
- (iv) the sum of a norm and a semi-norm is a norm,
- (v) and, finally, by taking into account *Lemma 1*.

$\square$

Now, as a direct consequence of *Lemmas 1* and *2* we have the following.

**Lemma 3.** Let  $(|\cdot|_l)_{l \in \{0, \dots, m\}}$  and  $(|\cdot|'_l)_{l \in \{0, \dots, m\}}$  be norm field collections, furthermore,  $\nabla$  and  $\nabla'$  be two covariant derivative operators as above. Then, there exists a positive  $C^r$  function  $C$  on  $M$  such that

$$\sum_{l=0}^r |\nabla'^{(l)} \cdot|_l \leq C \sum_{l=0}^r |\nabla^{(l)} \cdot|_l. \quad (\text{A.7})$$

Being armed with the above results we can turn to the generalization of Sobolev embedding theorem to compact Riemann manifolds.

**Theorem 4.** The Sobolev embedding theorem applies to compact Riemann manifolds, i.e., whenever  $M$  is a compact Riemann manifold of dimension  $n$  and  $r > \frac{n}{2} + k$  for non-negative integers  $r$  and  $k$ , the relation

$$H_r^2(M, \mathbb{C}) \subset C_\infty^k(M, \mathbb{C}) \quad (\text{A.8})$$

holds, and also there exists a positive real constant  $C$  such that the inequality

$$\|\cdot\|_{C_\infty^k(M, \mathbb{C})} \leq C \|\cdot\|_{H_r^2(M, \mathbb{C})} \quad (\text{A.9})$$

is satisfied.

*Proof.* Obviously, the inclusion (A.8) holds as an immediate consequence of the relevant differentiability assumptions, and because  $C_\infty^k(M, \mathbb{C}) = C_b^k(M, \mathbb{C}) = C^k(M, \mathbb{C})$  due to the compactness of  $M$ .

To justify (A.9) choose an arbitrary finite atlas  $\mathcal{A} = \{(U_i, \varphi_i) | i \in I\}$  of  $M$  with partition of unity  $\{\mathcal{F}_i | i \in I\}$  subordinate to it. In proceeding, choose a real number  $\varepsilon$  such that  $0 < \varepsilon \leq 1$ , and denote by  $V_i^\varepsilon$  the pre-image of the interval  $[\varepsilon, 1]$  by the map  $\mathcal{F}_i$  for each  $i \in I$ . Then, by applying the conventional Sobolev theorem over each compact set  $V_i^\varepsilon \subset \text{supp}(\mathcal{F}_i) \subset U_i$  we have that

$$\sup_{V_i^\varepsilon} \left( \sum_{l=0}^k |\nabla^{(l)} f| \right)^2 \leq C_i \sum_{l=0}^r \int_{V_i^\varepsilon} |\nabla^{(l)} f|^2 \quad (\text{A.10})$$

for any  $f \in H_r^2(M, \mathbb{C})$ , where now  $|\cdot|$ ,  $\nabla$  and the volume form are assumed to be determined by the Euclidean metric associated with the local coordinates,  $\varphi_i(U_i) \subset \mathbb{R}^n$ , on  $U_i$ . In virtue of *Lemma 3*, one may replace the Euclidean  $|\cdot|$ ,  $\nabla$  and the volume form with the norm, covariant derivation and the volume form determined by the Riemannian metric  $g$  on  $M$  with the understanding that, as a compensation, the values of Sobolev constants  $C_i$  have to be adjusted accordingly. Furthermore, as  $\mathcal{F}_i \geq \varepsilon$  over  $V_i^\varepsilon$ , we also have that

$$\sup_{V_i^\varepsilon} \left( \sum_{l=0}^k |\nabla^{(l)} f| \right)^2 \leq C_i \frac{1}{\varepsilon} \sum_{l=0}^r \int_{V_i^\varepsilon} \mathcal{F}_i |\nabla^{(l)} f|^2, \quad (\text{A.11})$$

where the monotonicity of the integral of a non-negative function has been taken into account. By making use of the above observations we also have that

$$\sum_{l=0}^r \int_M |\nabla^{(l)} f|^2 = \sum_{i \in I} \sum_{l=0}^r \int_{U_i} \mathcal{F}_i |\nabla^{(l)} f|^2$$

$$\begin{aligned}
 &\geq \sum_{i \in I} \sum_{l=0}^r \int_{V_i^\varepsilon} \mathcal{F}_i |\nabla^{(l)} f|^2 \\
 &\geq \sum_{i \in I} \frac{\varepsilon}{C_i} \sup_{V_i^\varepsilon} \left( \sum_{l=0}^k |\nabla^{(l)} f| \right)^2.
 \end{aligned} \tag{A.12}$$

This is exactly the point where we utilize the compactness of  $M$ . Accordingly, for the rest of the proof we shall assume that the index set  $I$  is finite, which immediately implies that for some positive constant  $C^\varepsilon$

$$\sum_{i \in I} \frac{\varepsilon}{C_i} \sup_{V_i^\varepsilon} \left( \sum_{l=0}^k |\nabla^{(l)} f| \right)^2 \geq C^\varepsilon \sup_{\bigcup_{i \in I} V_i^\varepsilon} \left( \sum_{l=0}^k |\nabla^{(l)} f| \right)^2 \tag{A.13}$$

holds. By choosing  $\varepsilon$  such that  $0 < \varepsilon \leq \frac{1}{|I|}$  we also have that  $\bigcup_{i \in I} V_i^\varepsilon = M$  since otherwise there would be a point  $p \in M$  so that  $\mathcal{F}_i(p) < \varepsilon$  for all  $i \in I$ . This, however, is impossible since then  $\sum_{i \in I} \mathcal{F}_i(p) < \sum_{i \in I} \varepsilon \leq 1$  would hold on contrary to the definition of the partition of unity. This, in virtue of (A.12) and (A.13), justify then that (A.9) holds.  $\square$

In applying the above results consider now a compact Riemann manifold  $M$ . As it is well-known [51] the eigenfunctions of the Laplace operator are in  $C_b^r(M, \mathbb{C})$ , and, more importantly, their linear span is dense in any of the Banach spaces  $C_b^l(M, \mathbb{C})$ , with  $0 \leq l \leq r$ . In addition,  $C_b^l(M, \mathbb{C}) \subset H_l^2(M, \mathbb{C})$  is dense and—in consequence of the Hölder's inequality—the  $C^l$  supremum norm is stronger than the  $H_l^2$  norm over compact manifolds. Therefore, the linear span of the Laplace eigenfunctions is dense in  $H_l^2(M, \mathbb{C})$ , and, in particular, in  $L^2(M, \mathbb{C})$ . It is also known that a linearly independent eigensystem of the Laplace operator over a compact manifold may be chosen to be orthonormal with respect to the  $L^2$  scalar product, hence these form a complete orthonormal system in  $L^2(M, \mathbb{C})$ , a complete orthogonal system in  $H_l^2(M, \mathbb{C})$ , as well as, a Schauder basis in  $C_b^l(M, \mathbb{C})$ , with  $0 \leq l \leq r$ . Let  $f \in H_r^2(M, \mathbb{C})$  be some function and  $\{Y_i\}_{i \in \mathcal{I}}$  be an  $L^2$ -orthonormal eigensystem of the Laplace operator. Then, as the elements of the system  $\{Y_i\}_{i \in \mathcal{I}}$  are eigenvectors of the Laplace operator, in virtue of the Gauss theorem, we have that

$$\langle Y_i, f \rangle_{H_r^2(M, \mathbb{C})} = \left( \sum_{l=0}^r (-\lambda_i)^l \right) \langle Y_i, f \rangle_{L^2(M, \mathbb{C})} \tag{A.14}$$

for each  $i \in \mathcal{I}$ , where  $\lambda_i$  denotes the associated eigenvalue, and  $\partial M = \emptyset$  has also been assumed. In order to simplify some of the succeeding expressions we introduce the function  $S_r : \mathbb{C} \rightarrow \mathbb{C}$  as

$$S_r(z) = \sum_{l=0}^r (-z)^l = \begin{cases} \frac{(-z)^{r+1}-1}{(-z)-1}, & \text{if } z \neq -1; \\ r+1, & \text{otherwise.} \end{cases} \tag{A.15}$$

As an immediate consequence of (A.14) the vector system  $\{Y_i/\sqrt{S_r(\lambda_i)}\}_{i \in \mathcal{I}}$  is orthonormal in  $H_r^2(M, \mathbb{C})$ . Therefore, for the series expansion of the function  $f$  in

$H_r^2(M, \mathbb{C})$  with respect to the complete orthonormal system  $\{Y_i/\sqrt{S_r(\lambda_i)}\}_{i \in \mathcal{I}}$

$$\sum_{i \in \mathcal{I}} \left\langle \frac{Y_i}{\sqrt{S_r(\lambda_i)}}, f \right\rangle_{H_r^2(M, \mathbb{C})} \cdot \frac{Y_i}{\sqrt{S_r(\lambda_i)}} = \sum_{i \in \mathcal{I}} \langle Y_i, f \rangle_{L^2(M, \mathbb{C})} Y_i, \quad (\text{A.16})$$

is satisfied, which relation implies then that the  $L^2$  series expansion of  $f$  with respect to  $\{Y_i\}_{i \in \mathcal{I}}$  is also convergent in the  $H_r^2$  sense.

By combining the above observations we have that whenever the assumptions of the Sobolev embedding theorem holds then the multipole series expansions—which are convergent in the  $L^2$  sense—will also be convergent in the uniform  $C^k$  sense.

**Corollary 5.** *Assume that  $f$  is a function that belongs to  $C^r(M, \mathbb{C})$ , where  $r > \frac{n}{2} + k$ . Then, the multipole series expansion of  $f$  with respect to an eigensystem  $\{Y_i\}_{i \in \mathcal{I}}$  of the Laplace operator is also convergent in the  $C^k$  sense. Furthermore, the convergence is independent of the summation order, as the system  $\{Y_i\}_{i \in \mathcal{I}}$  shall remain to be a complete orthogonal system in  $L^2(M, \mathbb{C})$  and in  $H_r^2(M, \mathbb{C})$  after any index permutation. Therefore, pointwise absolute convergence of the multipole series also follows for the derivatives up to the order  $k$ , as the absolute convergence in a finite dimensional Banach space (which is nothing but  $\mathbb{C}$  in the present case) is equivalent to summation order independent convergence.*

*Remark 6.* It is worth keeping in mind that the Schauder basis property of the Laplace eigenfunctions in  $C_b^k(M, \mathbb{C})$  does not guarantee that an arbitrary function  $f \in C_b^k(M, \mathbb{C})$  can always be expanded in the form of  $f = \sum_{i \in \mathcal{I}} f_i Y_i$ . (If that was true the relation  $f_i = \langle Y_i, f \rangle_{L^2}$ ,  $i \in \mathcal{I}$ , would immediately follow from Lebesgue's theorem of dominated convergence.) Our statement follows from the fact that whenever  $\{Y_i | i \in \mathcal{I}\}$  is a Schauder basis that guarantees merely that the linear span of this system is dense in  $C_b^k(M, \mathbb{C})$ , i.e. every field  $f$  may be approximated by a sequence of finite linear combinations of this basis. This means that the series expandability with respect to a Schauder basis follows automatically only in Hilbert spaces, but not in general in Banach spaces.

It is important to emphasize that the pointwise absolute convergence property plays a crucial role in non-linear problems. To see this note that whenever the conditions of the above corollary are guaranteed to hold the pointwise product  $f \cdot g$  of multipole expansions  $f = \sum_{i \in \mathcal{I}} f_i Y_i$  and  $g = \sum_{i \in \mathcal{I}} g_i Y_i$  may be written in the optimal form

$$f \cdot g = \left( \sum_{i \in \mathcal{I}} f_i Y_i \right) \left( \sum_{j \in \mathcal{I}} g_j Y_j \right) = \sum_{i, j \in \mathcal{I}} f_i g_j \cdot Y_i Y_j, \quad (\text{A.17})$$

where the sums are understood in the pointwise manner, which, due to Fubini's theorem, are absolute convergent along with their derivatives up to the order  $k$ . The sums may also be understood in the uniform  $C^k$  manner independently of the summation order, however, in this case we do not get *absolute* uniform  $C^k$  convergence.

The most significant advantages associated with the use of multipole analysis manifest themselves in evaluating non-linear terms. In fact, whenever the pointwise

absolute convergence is guaranteed for  $f \cdot g$  we have that

$$f \cdot g = \sum_{k \in \mathcal{I}} (f \cdot g)_k Y_k, \quad (\text{A.18})$$

where

$$\begin{aligned} (f \cdot g)_k &= \langle Y_k, f \cdot g \rangle \\ &= \int_M \bar{Y}_k \left( \sum_{i \in \mathcal{I}} f_i Y_i \right) \left( \sum_{j \in \mathcal{I}} g_j Y_j \right) \\ &= \sum_{i \in \mathcal{I}} \sum_{j \in \mathcal{I}} f_i g_j \int_M \bar{Y}_k Y_i Y_j. \end{aligned} \quad (\text{A.19})$$

In deriving (A.19) we have used that, in virtue of Lebesgue's dominated convergence theorem, the summation and the integration can be interchanged, and also that the double sums are known to be uniformly convergent. Therefore, whenever the matrix elements  $\int Y_i Y_j Y_k$  with  $i, j, k \in \mathcal{I}$ , which are also known as Gaunt coefficients, can be determined, then, the multipole series expansion on multi-linear expressions may constructively be evaluated by making use of the multipole expansion of its factors.

## Appendix B. The Explicit Form of Gaunt Coefficients on Two-sphere and on $n$ -dimensional Torus

It is known (see, e.g., [52, 53]) that the Gaunt coefficients on a two-sphere,  $\mathbb{S}^2$ , may be given either in terms of the Wigner 3j symbols or in terms of the Clebsch-Gordan coefficients. It is also known that the Clebsch-Gordan coefficients can be evaluated by various numerical algorithms, e.g., by the Racah formula [54] (see also [55]).

In providing the Gaunt coefficients let us denote the spherical harmonics, which comprises the familiar orthonormal basis, by  $Y_\ell^m$  with integers  $\ell, m$  satisfying the relations  $0 \leq \ell < \infty$  and  $-\ell \leq m \leq \ell$ .

Then, the Gaunt coefficient  $\int_{\mathbb{S}^2} Y_{\ell_1}^{m_1} Y_{\ell_2}^{m_2} Y_{\ell_3}^{m_3}$  is known to be zero if either of the following conditions holds

- (i)  $m_1 + m_2 + m_3 \neq 0$ , or
- (ii)  $\ell_3 < |\ell_1 - \ell_2|$  or  $\ell_1 + \ell_2 < \ell_3$ , or
- (iii)  $\ell_1 + \ell_2 + \ell_3$  is odd.

The Gaunt coefficients may also be related to the Wigner 3j symbols as

$$\begin{aligned} &\int_{\mathbb{S}^2} Y_{\ell_1}^{m_1} Y_{\ell_2}^{m_2} Y_{\ell_3}^{m_3} \\ &= \sqrt{\frac{(2\ell_1 + 1)(2\ell_2 + 1)(2\ell_3 + 1)}{4\pi}} \cdot \begin{pmatrix} \ell_1 & \ell_2 & \ell_3 \\ 0 & 0 & 0 \end{pmatrix} \begin{pmatrix} \ell_1 & \ell_2 & \ell_3 \\ m_1 & m_2 & m_3 \end{pmatrix}, \end{aligned} \quad (\text{B.1})$$

where the Wigner 3j symbols are given by the Clebsch-Gordan coefficients as

$$\begin{pmatrix} \ell_1 & \ell_2 & \ell_3 \\ m_1 & m_2 & m_3 \end{pmatrix} = \frac{(-1)^{-m_3 + \ell_1 - \ell_2}}{\sqrt{2\ell_3 + 1}} \cdot (\ell_1 \ell_2 m_1 m_2 | \ell_1 \ell_2 \ell_3 (-m_3)). \quad (\text{B.2})$$



The Gaunt coefficients relevant for the case of an  $n$ -dimensional torus,  $\mathbb{T}^n$ , are known to possess an even simpler structure. By making use of the orthonormal eigenstates  $Y_{k^1, \dots, k^n}$ , labeled by the integers  $k^1, \dots, k^n$  of the Laplace operator on  $\mathbb{T}^n$ , the integrals  $\int_{\mathbb{T}^n} Y_{k_1^1, \dots, k_1^n} \cdot Y_{k_2^1, \dots, k_2^n} \cdot Y_{k_3^1, \dots, k_3^n}$  may be seen to be zero if there exists  $i \in \{1, \dots, n\}$  such that  $k_1^i + k_2^i + k_3^i \neq 0$  while it is  $\frac{1}{(\sqrt{2\pi})^n}$  otherwise.

### Appendix C. The Division as an Operation within the Framework of Multipole Expansions

One of the most delicate issues while using multipole expansions arises whenever we have expressions containing the operation of division by a function. Clearly, if this function vanishes somewhere, then, a direct evaluation of the division is not tolerated by any of the numerical methods. However, if this function is guaranteed to be bounded and nowhere zero, then both the multiplication and the division by it are continuous operations in either of the function spaces  $L^2$ ,  $C_b^k$  and  $H_k^2$  with the understanding that in the latter two cases the result belongs to the corresponding spaces if the function itself belongs to  $C_b^k$ . In the latter case, by making use of the Neumann series expansion the action of the division operator may be traced back to the multiple use of the multiplication operator.

To justify our last claim consider first a continuous operator  $A$  acting on a Banach space with identity operator  $I$ . It is straightforward to check then, by induction, that

$$A \sum_{i=0}^N (I - A)^i = \sum_{i=0}^N (I - A)^i A = I - (I - A)^{N+1} \quad (\text{C.1})$$

holds for arbitrary non-negative integer  $N$ . If  $\|I - A\| < 1$  we also have that the series  $N \mapsto \sum_{i=0}^N (I - A)^i$  is absolute convergent (thus its limit is a continuous operator), and  $\|(I - A)^{N+1}\| \leq \|I - A\|^{N+1}$  tends to zero as  $N \rightarrow \infty$ . Thus the relation  $A^{-1} = \sum_{i=0}^{\infty} (I - A)^i$ —referred as the Neumann series expansion—follows. Assume now that the Banach space in question is  $C_b^k(M, \mathbb{C})$ , and the operator  $A$  is the multiplication by a function  $F \in C_b^k(M, \mathbb{C})$ , and denote by  $\|I - F\|$  the pertinent operator norm of the function  $1 - F$ . Accordingly, an upper bound for the error that we introduce by replacing the division operation by multiplication based on the Neumann series may be given as

$$\begin{aligned} & \left\| 1 - F \sum_{i=0}^N (1 - F)^i \right\| = \left\| 1 - \sum_{i=0}^N (1 - F)^i F \right\| \\ & \leq \|1 - F\|_{C_b^k}^{N+1}. \end{aligned} \quad (\text{C.2})$$

When  $F$  is specified by its multipole coefficients, it is not economical to determine the  $C_b^k$  norm of  $1 - F$ , as it would require pointwise evaluation of its multipole series. However, if  $F \in C_b^r$  for  $r > \frac{n}{2} + k$ , and our Riemann manifold is compact, the Sobolev embedding theorem significantly simplifies the determination of an upper bound of the uniform  $C^k$

norm as

$$\|1 - F\|_{C_b^k} = \|1 - F\|_{C_\infty^k} \leq C \|1 - F\|_{H_r^2}, \quad (\text{C.3})$$

where  $C$  is the minimal Sobolev constant, and the Sobolev norm on the right hand side may directly be determined by making use of the multipole coefficients of  $F$  as

$$\sqrt{\sum_{i \in \mathcal{I}} S_r(\lambda_i) |\langle Y_i, 1 \rangle_{L^2} - \langle Y_i, F \rangle_{L^2}|^2} \quad (\text{C.4})$$

where the function  $S_r$  introduced in Appendix A has been applied. Given the value of  $C \|1 - F\|_{H_r^2} < 1$ , a predefined error tolerance  $\varepsilon$  can be guaranteed to hold simply by calculating Neumann series up to the order  $N_\varepsilon = \text{int} \{ \ln(\varepsilon) / \ln(C \|1 - F\|_{H_r^2}) \}$ , where  $\text{int} \{x\}$  denotes the integer part of  $x \in \mathbb{R}$ . It is straightforward to see that the number of orders to be calculated grows only logarithmically with the increase of the desired accuracy.

The above described method based on the use of the Neumann series may further be optimized by rescaling our field  $F$  with a complex number  $z$  in a way to minimize  $(\|1 - zF\|_{H_r^2})^2$ . It can be justified, by a direct calculation, that the unique minimum may be achieved by choosing

$$z(F) = \frac{\sum_{i \in \mathcal{I}} S_r(\lambda_i) \overline{\langle Y_i, F \rangle_{L^2}} \langle Y_i, 1 \rangle_{L^2}}{\sum_{j \in \mathcal{I}} S_r(\lambda_j) |\langle Y_j, F \rangle_{L^2}|^2}, \quad (\text{C.5})$$

and the corresponding minimal value is

$$M(F) = \sum_{i \in \mathcal{I}} S_r(\lambda_i) |\langle Y_i, 1 \rangle_{L^2}|^2 - \frac{\left| \sum_{j \in \mathcal{I}} S_r(\lambda_j) \overline{\langle Y_j, F \rangle_{L^2}} \langle Y_j, 1 \rangle_{L^2} \right|^2}{\sum_{k \in \mathcal{I}} S_r(\lambda_k) |\langle Y_k, F \rangle_{L^2}|^2}. \quad (\text{C.6})$$

If we denote the constant eigenfunction of the Laplace operator by  $Y_0$ , then  $z(F)$  and  $M(F)$  can be re-expressed as  $z(F) = \frac{1}{Y_0} \frac{\overline{\langle Y_0, F \rangle_{L^2}}}{\|F\|_{H_r^2}^2}$  and  $M(F) = \frac{1}{|Y_0|^2} \frac{\|F - \langle Y_0, F \rangle_{L^2} Y_0\|_{H_r^2}^2}{\|F\|_{H_r^2}^2}$ . If optimal rescaling is applied, a sufficient condition for the Neumann series to converge is that the inequality  $C \cdot \sqrt{M(F)} < 1$ , where  $C$  stands for the Sobolev constant, holds and the minimum number of orders necessary to achieve an accuracy below a pre-fixed value  $\varepsilon$  is  $N_\varepsilon = \text{int} \{ \ln(\varepsilon) / \ln(C \sqrt{M(F)}) \}$ . This requirement may also be rephrased as follows. The Neumann series after optimal rescaling is absolute convergent in the uniform  $C^k$  norm if  $\frac{\|F - \langle Y_0, F \rangle_{L^2} Y_0\|_{H_r^2}}{\|F\|_{H_r^2}}$ —which is nothing but the  $H_r^2$ -measure of the non-monopole content in  $F$ —is smaller than the threshold  $\frac{|Y_0|}{C}$ . As it will be demonstrated by the following two examples relevant for the case of the two-spheres and  $n$ -dimensional toruses, this is a rather weak condition. It is also worth to note that the Neumann series expansion may be re-expressed in an iterative form, which requires less function evaluations than the canonical series expansion representation does [56].

## Appendix D. The Sobolev Constants on Two-sphere and on $n$ -Toruses

As it follows from the discussions in Appendix C, to be able to have accurate estimates of certain errors, it is also important to know the numerical value of the minimal Sobolev

constant. In general, the determination of the value of the minimal Sobolev constant is a delicate issue. A powerful method yielding this constant is based on the use of *reproducing kernel property* [57] of Sobolev spaces which can be outlined as follows. Consider a Hilbert space  $\mathcal{H}$  of some complex valued functions over some set  $X$ . Then, if the point evaluation  $f \mapsto f(x)$  is a continuous linear map for every  $x \in X$  it is called a reproducing kernel Hilbert space. The Riesz representation theorem ensures that for each  $x \in X$  there exists a unique  $K_x \in \mathcal{H}$  such that  $\langle K_x, f \rangle = f(x)$  for any  $f \in \mathcal{H}$ . As  $K_x$  itself is a function, it may also be evaluated at any point. The reproducing kernel function  $K : X \times X \mapsto \mathbb{C}$  is defined as  $K(x, y) = K_x(y)$ . It may be verified that for any  $x, y \in X$

- (i)  $\langle K(x, \cdot), K(y, \cdot) \rangle = K(y, x)$ ,
- (ii)  $\bar{K}(y, x) = K(x, y)$ ,
- (iii) if  $(\Phi_i)_{i \in \mathcal{I}}$  comprises a complete orthonormal system, then,  $K(x, \cdot) = \sum_{i \in \mathcal{I}} \bar{\Phi}_i(x) \Phi_i$ , where the infinite summation makes sense in the norm topology.

If  $H_r^2(M, \mathbb{C})$  is a Sobolev space over a compact Riemann manifold  $M$  with  $r > \frac{n}{2} + k$ , then by the Sobolev theorem the  $H_r^2$  norm is stronger than the uniform  $C^k$  norm, therefore the point evaluation is a continuous map. Thus, for an arbitrary choice of an  $L^2$ -orthonormal eigensystem  $\{Y_i\}_{i \in \mathcal{I}}$  of the Laplace operator, there exists a unique reproducing kernel function  $K_r$  which—for any choice of  $x \in M$  reads—as  $K_r(x, \cdot) = \sum_{i \in \mathcal{I}} \frac{1}{s_r(\lambda_i)} \bar{Y}_i(x) Y_i$ , and for any  $f \in H_r^2(M, \mathbb{C})$  we have  $\langle K_r(x, \cdot), f \rangle_{H_r^2(M, \mathbb{C})} = f(x)$ . Armed with this identity, the relation

$$\langle ((\nabla^{(l)} \otimes \text{id}) K_r)(x, \cdot), f \rangle_{H_r^2(M, \mathbb{C})} = (\nabla^{(l)} f)(x) \quad (\text{D.1})$$

can be seen to hold, where the operator  $(\nabla^{(l)} \otimes \text{id})$  acts on  $K_r$  as the  $l$ -times gradient—with  $l = 0, \dots, k$ —on the first variable of  $K_r$  while the second variable of  $K_r$  remains intact. Note that, in virtue of Lebesgue's dominated convergence theorem, the order of the action of the gradient  $\nabla$  and the scalar product  $\langle \cdot, \cdot \rangle$  may be interchanged. All these observations imply that

$$\begin{aligned} & |\nabla^{(l)} f|(x) \\ &= \left| \langle ((\nabla^{(l)} \otimes \text{id}) K_r)(x, \cdot), f \rangle_{H_r^2(M, \mathbb{C})} \right| \\ &\leq \|((\nabla^{(l)} \otimes \text{id}) K_r)(x, \cdot)\|_{H_r^2(M, \mathbb{C})} \|f\|_{H_r^2(M, \mathbb{C})}, \end{aligned} \quad (\text{D.2})$$

where in the second step the Cauchy-Schwartz inequality in  $H_r^2(M, \mathbb{C})$  has been applied. This inequality is known to be sharp, i.e. it may be saturated. When the norm  $\|((\nabla^{(l)} \otimes \text{id}) K_r)(x, \cdot)\|_{H_r^2(M, \mathbb{C})}$  is guaranteed to be independent of  $x \in M$ —this happens, e.g. in case of homogeneous manifolds—we get the sharp inequality

$$\sup_{x \in M} |\nabla^{(l)} f|(x) \leq \sup_{x \in M} \|((\nabla^{(l)} \otimes \text{id}) K_r)(x, \cdot)\|_{H_r^2(M, \mathbb{C})} \|f\|_{H_r^2(M, \mathbb{C})}. \quad (\text{D.3})$$

Applying this relation to the case of  $k = 0$  the minimal Sobolev constant may be read off the particular form of (D.3) as

$$\|f\|_{C^0} \leq \sup_{x \in M} \|K_r(x, \cdot)\|_{H_r^2(M, \mathbb{C})} \|f\|_{H_r^2(M, \mathbb{C})}, \quad (\text{D.4})$$

where  $r > \frac{n}{2}$  is tacitly assumed to hold. Note, however, that for higher value of  $k$  the above argument does not necessarily lead to a sharp inequality.

Let us restrict again considerations to the case of a two-sphere where, according to the above discussion, the reproducing kernel can be given as

$$K_r(x, \cdot) = \sum_{\ell=0}^{\infty} \sum_{m=-\ell}^{\ell} \frac{\ell(\ell+1) - 1}{(\ell(\ell+1))^{r+1} - 1} \bar{Y}_{\ell}^m(x) Y_{\ell}^m. \quad (\text{D.5})$$

Then, as the two-sphere is a homogeneous manifold  $\|((\nabla^{(\ell)} \otimes \text{id}) K_r)(x, \cdot)\|_{H_r^2(M, \mathbb{C})}$  is independent of the location of  $x$  on  $\mathbb{S}^2$ . By choosing  $x$  to be the north pole in standard spherical polar coordinates, and also by using the values of the spherical harmonics at the north pole we immediately get that

$$\|K_r(x, \cdot)\|_{H_r^2}^2 = \frac{1}{4\pi} \sum_{\ell=0}^{\infty} \frac{(2\ell+1)(\ell(\ell+1) - 1)}{(\ell(\ell+1))^{r+1} - 1}. \quad (\text{D.6})$$

The square root of the right hand side of (D.6) provides the minimal value of the Sobolev constant,  $C_r$ , over the two-sphere with  $k = 0$  and  $r > 1$ . The approximate numerical values of this Sobolev constants  $C_r$  for the particular values of  $r = 2, 3, 4$  are listed in Table D1.

$r$	Sobolev constant
2	$\frac{1}{\sqrt{4\pi}} \cdot 1.284533$
3	$\frac{1}{\sqrt{4\pi}} \cdot 1.106732$
4	$\frac{1}{\sqrt{4\pi}} \cdot 1.048986$

**Table D1.** Approximate values of the minimal Sobolev constant in the  $C^0 \subset H_r^2$  Sobolev embedding over the two-sphere, for the  $r = 2, 3, 4$  values.

Let us finally restrict attention to the case of an  $n$ -dimensional torus. Then, the reproducing kernel may be given as

$$K_r(x, \cdot) = \sum_{k_1=-\infty}^{+\infty} \dots \sum_{k_n=-\infty}^{+\infty} \frac{\bar{Y}_{k_1, \dots, k_n}(x) \cdot Y_{k_1, \dots, k_n}}{S_r(-k_1^2 - \dots - k_n^2)}, \quad (\text{D.7})$$

where  $\|((\nabla^{(\ell)} \otimes \text{id}) K_r)(x, \cdot)\|_{H_r^2}$  is constant as a function of  $x \in \mathbb{T}^n$ , as the  $n$ -torus is also a homogeneous manifold. By choosing  $x$  to be the point where all the polar angle coordinates are zero we immediately get

$$\|K_r(x, \cdot)\|_{H_r^2}^2 = \frac{1}{(2\pi)^n} \sum_{k_1=-\infty}^{+\infty} \dots \sum_{k_n=-\infty}^{+\infty} \frac{1}{S_r(-k_1^2 - \dots - k_n^2)}. \quad (\text{D.8})$$

The square root of this expression gives the minimal Sobolev constants,  $C_r$ , for the Sobolev inequality with  $r > \frac{n}{2}$  and  $k = 0$ . For the particular case of  $\mathbb{T}^2$ , the approximate numerical value of the Sobolev constants  $C_r$  for  $k = 0$  and for the particular values of  $r = 2, 3, 4$  are listed in Table D2.

$r$	Sobolev constant
2	$\frac{1}{2\pi} \cdot 1.943685$
3	$\frac{1}{2\pi} \cdot 1.547391$
4	$\frac{1}{2\pi} \cdot 1.397749$

**Table D2.** Approximate values of the minimal Sobolev constant in the  $C^0 \subset H_r^2$  Sobolev embedding over the two-torus, for the  $r = 2, 3, 4$  values.

## Appendix E. The Estimation of the Tail Sum Error

As our numerical method is based on the use of multipole expansion of the basic field variables, and also since, in practice, we always use only a finite number of multipole components, it is of crucial importance to provide precise estimates on the pertinent errors. An immediate upper bound on the Sobolev norm of the truncated part of a function  $f$  may be given as follows.

Let  $f \in H_r^2(M, \mathbb{C})$  for some  $r$ , then, in virtue of (A.14), we have that

$$\sum_{i \in \mathcal{I}} S_r(\lambda_i) |\langle Y_i, f \rangle_{L^2}|^2 = \|f\|_{H_r^2}^2 < \infty, \quad (\text{E.1})$$

which implies that the sequence  $i \mapsto S_r(\lambda_i) |\langle Y_i, f \rangle_{L^2}|^2$  is summable. Consider now a sequence of positive numbers  $i \mapsto a_i$  such that the relation

$$|\langle Y_i, f \rangle_{L^2}| \leq a_i \quad (\text{E.2})$$

holds for each  $i \in \mathcal{I}$ . Then, because the summation preserves monotonicity, the tail sum of the sequence  $i \mapsto S_r(\lambda_i) |a_i|^2$  bounds the  $H_r^2$  norm-square of the tail sum error of  $f$ . Such a bounding sequence may be readily constructed by assuming that  $f \in H_{r'}^2(M, \mathbb{C})$  for some  $r' > r$ , which implies that also

$$\sum_{i \in \mathcal{I}} S_{r'}(\lambda_i) |\langle Y_i, f \rangle_{L^2}|^2 = \|f\|_{H_{r'}^2}^2 < \infty \quad (\text{E.3})$$

holds. Then, the sequence  $i \mapsto a_i$  may be chosen to be an arbitrary monotonically decreasing sequence, for which the sum  $\sum_{i \in \mathcal{I}} S_{r'}(\lambda_i) |a_i|^2$  is divergent, as in that case, there always exists a threshold index, above which the relation (E.2) holds. Then,  $i \mapsto a_i$  may be normalized in such a way that (E.2) holds for any  $i \in \mathcal{I}$ . Such a minimal multiplier would be  $\max_{i \in \mathcal{I}} \frac{1}{a_i} |\langle Y_i, f \rangle|$ , which, in practice, may always be identified by the pertinent maximum on the stored finite orders. Note that this approximation is exact whenever the threshold index is reached within the stored orders.

Restricting again considerations to the case of a two-sphere, a suitable bounding sequence  $(\ell, m) \mapsto a_\ell^m$  may be chosen as

$$(\ell, m) \mapsto K \frac{1}{2\ell + 1} \left( \frac{(\ell(\ell + 1))^{r'+1} - 1}{(\ell(\ell + 1)) - 1} \right)^{-1/2}, \quad (\text{E.4})$$

where  $K$  is an unknown normalization factor. Then, the inequality

$$\sum_{\ell=\ell_{\max}+1}^{\infty} \sum_{m=-\ell}^{\ell} \frac{(\ell(\ell + 1))^{r'+1} - 1}{(\ell(\ell + 1)) - 1} |\langle Y_\ell^m, f \rangle_{L^2}|^2$$

$$\leq |K|^2 \sum_{\ell=\ell_{\max}+1}^{\infty} \frac{(\ell(\ell+1))^{r'+1} - 1}{(\ell(\ell+1))^{r'+1} - 1} \frac{1}{2\ell+1} \quad (\text{E.5})$$

holds for the  $H_r^2$  norm-square of the tail sum, whenever  $|K|$  is chosen to be large enough such that the inequality  $|\langle Y_\ell^m, f \rangle_{L^2}| \leq |K| \frac{1}{2\ell+1} \left( \frac{(\ell(\ell+1))^{r'+1} - 1}{(\ell(\ell+1)) - 1} \right)^{-1/2}$  is satisfied for any allowed values of  $\ell, m$ , where  $r < r'$ . An immediate lower bound for such  $|K|$  may be given as

$$\max_{\ell=0, \dots, \infty} \max_{m=-\ell, \dots, \ell} \sqrt{\frac{(\ell(\ell+1))^{r'+1} - 1}{(\ell(\ell+1)) - 1}} (2\ell+1) |\langle Y_\ell^m, f \rangle_{L^2}|. \quad (\text{E.6})$$

By construction, the maximum value in question is necessarily attained at certain finite but unspecified  $\ell$ . In numerical applications, an estimate for  $|K|$  may be obtained by assuming that the stored components up to the order  $\ell_{\max}$  already encode the relevant multipole orders for the field, i.e., the multipole coefficients in the tail already fit into the above scheme of the asymptotics. In this case, we may choose  $K$  as

$$K = \max_{\ell=0, \dots, \ell_{\max}} \max_{m=-\ell, \dots, \ell} \sqrt{\frac{(\ell(\ell+1))^{r'+1} - 1}{(\ell(\ell+1)) - 1}} (2\ell+1) |\langle Y_\ell^m, f \rangle_{L^2}|. \quad (\text{E.7})$$

It follows from the above observations that whenever  $f \in C^\infty(\mathbb{S}^2, \mathbb{C})$  then—since for any  $r' f \in H_r^2(\mathbb{S}^2, \mathbb{C})$  also holds—its multipole coefficients  $\langle Y_\ell^m, f \rangle_{L^2}$  shall decay faster than any polynomial in  $\ell$ . Note finally, that this upper bound on the  $H_r^2$  norm of the tail sum error may be used, along with the Sobolev constant, to derive an upper bound on the  $C^0$  norm of the tail sum error.

## Appendix F. The Evaluation of the Integrals determining Radiation Anisotropy

In various physical applications it is important to determine the flux of conserved quantities through a hypersurface with topology  $\mathbb{R} \times \mathcal{C}$ .

In the applied framework of multipole expansions the calculation of these type of quantities is rather straightforward, as, in general, they may be written as integrals of multilinear expressions of the basic variables over the compact surface  $\mathcal{C}$ . Thereby they can be given in terms of  $L^2(\mathcal{C}, \mathbb{C})$  scalar products of some of the multilinear expressions of the basic field variables. Recall that multilinear expressions may be evaluated by purely spectral methods—as pointed out in Appendix A and Appendix B—, whereas the  $L^2$  scalar product may be calculated directly, using the fact that the eigenfunctions of the Laplace operator comprise an orthonormal system.

However, when we are interested in the scale of the anisotropy in the distribution of certain quantities, e.g. the energy radiated inwards or outwards, which cannot be expressed via the aforementioned integrals over the entire compact surface  $\mathcal{C}$ . Instead, the pertinent integrals have to be evaluated over a subset  $\mathcal{A} \subset \mathcal{C}$  to compare the radiated flux through  $\mathcal{A}$  and its complement in  $\mathcal{C}$ . These type of integrals may, however, be given as  $\langle \cdot, \chi_{\mathcal{A}} \cdot \rangle_{L^2(\mathcal{C}, \mathbb{C})}$  scalar products of multilinear expressions of basic field variables over

$\mathcal{C}$ , where  $\chi_{\mathcal{A}}$  denotes the characteristic function of the set  $\mathcal{A}$ . As the multiplication by  $\chi_{\mathcal{A}}$  is a continuous map, all that we need for the spectral evaluation of this expression is the values of the  $\langle Y_i, \chi_{\mathcal{A}} Y_j \rangle_{L^2(\mathcal{C}, \mathbb{C})}$  ( $i, j \in \mathcal{I}$ ) matrix elements.

To demonstrate that this process is much more straightforward in practice than it sounds let us restrict our considerations again to the case of the two-sphere. Then we have that

$$\begin{aligned} \langle Y_{\ell_1}^{m_1}, \chi_{\mathcal{A}} Y_{\ell_2}^{m_2} \rangle_{L^2} &= \int_{\mathcal{A}} \bar{Y}_{\ell_1}^{m_1} Y_{\ell_2}^{m_2} \\ &= (-1)^{m_2} \sum_{k=0}^{\min(\ell_1, \ell_2)} G_{\ell_1, \ell_2, |\ell_1 - \ell_2| + 2k}^{-m_1, m_2, -(m_2 - m_1)} \int_{\mathcal{A}} Y_{|\ell_1 - \ell_2| + 2k}^{m_2 - m_1}, \end{aligned} \quad (\text{F.1})$$

where the expansion of products of spherical harmonics was used, and the symbol  $G$  stands for the Gaunt coefficients (B.1).

Let us further restrict considerations to an axially symmetric subset  $\mathcal{A} \subset \mathcal{C}$ . Then, in our parametrization, the integral  $\int_{\mathcal{A}} Y_{|\ell_1 - \ell_2| + 2k}^{m_2 - m_1}$  vanishes, unless  $m_2 = m_1$ . Moreover, the integral  $\int_{\mathcal{A}} Y_{|\ell_1 - \ell_2| + 2k}^0$  may be calculated by making use of the identity

$$P'_{\ell+1} - P'_{\ell-1} = (2\ell + 1)P_{\ell}. \quad (\text{F.2})$$

This relation, which is valid for Legendre polynomials, may easily be verified by using the Rodriguez formula. As a consequence, the relation

$$\int_{[0, \vartheta] \times [0, 2\pi]} Y_{\ell}^0 = \sqrt{\pi} \delta_{\ell, 0} - \sqrt{\frac{\pi}{2\ell + 1}} [P_{\ell+1}(\cos \vartheta) - P_{\ell-1}(\cos \vartheta)] \quad (\text{F.3})$$

holds, where  $\delta$  denotes Kronecker delta. Note that in evaluating the Legendre polynomials well-known computational methods can be applied (for a relevant implementation see, e.g. [55]).

## References

- [1] Pretorius F 2005 Evolution of binary black hole spacetimes *Phys. Rev. Lett.* **95** 121101
- [2] Campanelli M, Lousto C O, Marronetti P and Zlochower Y 2006 Accurate evolutions of orbiting black hole binaries without excision *Phys. Rev. Lett.* **96** 111101
- [3] Baker J G, Centrella J, Choi D I, Koppitz M and van Meter J 2006 Gravitational wave extraction from an inspiraling configuration of merging black holes *Phys. Rev. Lett.* **96** 111102
- [4] Shibata M and Nakamura T 1995 Evolution of three-dimensional gravitational waves: Harmonic slicing case *Phys. Rev. D* **52** 5428–5444
- [5] Baumgarte T W and Shapiro S L 1999 On the numerical integration of Einstein's field equations *Phys. Rev. D* **59** 024007
- [6] Löffler F, Faber J, Bentivegna E, Bode T, Diener P, Haas R, Hinder I, Mundim B C, Ott C D, Schnetter E, Allen G, Campanelli M and Laguna P 2011 The Einstein toolkit: a community computational infrastructure for relativistic astrophysics *Preprint* gr-qc/1111.3344
- [7] Shibata M and Taniguchi K 2011 Coalescence of black hole-neutron star binaries <http://www.livingreviews.org/lrr-2011-6>
- [8] Burko L M and Khanna G 2009 Late-time Kerr Tails Revisited *Class. Quantum Grav.* **26** 015014
- [9] Tiglio M, Kidder L and Teukolsky S A 2008 High accuracy simulations of Kerr tails: coordinate dependence and higher multipoles *Class. Quantum Grav.* **25** 105022

- [10] Scheel M A, Erickcek A L, Burko L M, Kidder L E, Pfeiffer H P and Teukolsky S A 2004 3D simulations of linearized scalar fields in Kerr spacetime *Phys. Rev. D* **69** 104006
- [11] Zenginoglu A and Tiglio M 2009 Spacelike matching to null infinity *Phys. Rev. D* **80** 024044
- [12] Zenginoglu A 2008 Hyperboloidal evolution with the Einstein equations *Class. Quantum Grav.* **25** 195025
- [13] Zenginoglu A and Kidder L E 2010 Hyperboloidal evolution of test fields in three spatial dimensions *Phys. Rev. D* **81** 124010
- [14] Robertshaw O 2011 A spectral MHD code for the non-linear study of magnetic neutron stars *PhD thesis*, University of Southampton
- [15] R acz I and T oth G Z 2011 Numerical investigation of the late-time Kerr tails *Class. Quantum Grav.* **28** 195003
- [16] Williams R K 2004 Collimated escaping vortical polar  $e^-e^+$  jets intrinsically produced by rotating black holes and Penrose processes *The Astrophys. J.* **611** 952
- [17] Gariel J, MacCallum A H, Marcilhacy G and Santos N O 2010 Kerr geodesics, the Penrose process and jet collimation by a black hole *Astronomy & Astrophysics* **515** A15
- [18] Takami K and Kojima Y 2009 Collimation of a spherical collisionless particles stream in Kerr spacetime *Class. Quantum Grav.* **26** 085013
- [19] Csizmadia P, L aszl o A and R acz I 2010 Linear waves on fixed Kerr background and their relevance in jet formation *Journ. Phys. Conf. Ser.* **218** 012007
- [20] The GridRipper 3+1d PDE solver homepage  
<http://www.rmki.kfki.hu/~gridripper>
- [21] Teukolsky S A 1972 Rotating Black Holes: Separable Wave Equations for Gravitational and Electromagnetic Perturbations *Phys. Rev. Lett.* **29**, 1114-1118
- [22] Press W H and Teukolsky S A 1973 Perturbations of a Rotating Black Hole. II. Dynamical Stability of the Kerr Metric *Astrophys. J.* **185**, 649-674
- [23] Rezzolla L, Giacomazzo B, Baiotti L, Granot J, Kouveliotou C and Aloy M A 2011 The Missing Link: Merging Neutron Stars Naturally Produce Jet-like Structures and Can Power Short Gamma-ray Bursts *Astrophys. J. Letters* **732** L6
- [24] Lehner L, Palenzuela C, Liebling S.L, Thompson C and Hanna C 2011 Intense Electromagnetic Outbursts from Collapsing Hypermassive Neutron Stars *Preprint gr-qc/1112.2622*
- [25] Etienne Z.B, Liu Y T, Paschalidis V and Shapiro S L 2012 General relativistic simulations of black hole-neutron star mergers: Effects of magnetic fields *Phys. Rev. D* **85** 064029
- [26] Gustafsson B, Kreiss H O and Oliger J 1995 Time dependent problems and difference methods *Pure and Applied Mathematics* (New York: Wiley)
- [27] Wald R M 1984 General relativity (Chicago: University of Chicago Press)
- [28] Chandrasekhar S 1983 The mathematical theory of black holes (Oxford: Oxford University Press)
- [29] Csizmadia P 2006 Testing a new mesh refinement code in the evolution of a spherically symmetric Klein-Gordon field *Int. J. Mod. Phys. D* **15** 107
- [30] Csizmadia P 2007 Fourth order AMR and nonlinear dynamical systems in compactified space *Class. Quantum Grav.* **24** S369
- [31] Berger M J and Oliger J 1984 Adaptive mesh refinement for hyperbolic partial differential equations *J. Comput. Phys.* **53** 484
- [32] Friedrich H and Nagy G 1999 The initial boundary value problem for Einstein's vacuum field equations *Commun. Math. Phys.* **201** 619-655
- [33] Friedrich H and Rendall A D 2000 The Cauchy problem for the Einstein equations *Lect. Notes Phys.* **540** 127-224
- [34] Dafermos M and Rodnianski I 2004 A note on boundary value problems for black hole evolution *Preprint gr-qc/0403034*
- [35] Friedrich H 2009 Initial boundary value problems for Einstein's field equations and geometric uniqueness *Gen. Rel. Grav.* **41** 1947-1966
- [36] Sarbach O 2007 Absorbing boundary conditions for Einstein's field equations *J. Phys. Conf. Ser.*



91 012005

- [37] Allen E W, Buckmiller E, Burko L M and Price R H 2004 Radiation tails and boundary conditions for black hole evolutions *Phys. Rev. D* **70** 044038
- [38] Cszimadia P and Rácz I 2010 Gravitational collapse and topology change in spherically symmetric dynamical systems *Class. Quantum Grav.* **27** 015001
- [39] Carter B 1968 Global structure of the Kerr family of gravitational fields *Phys. Rev.* **174** 1559
- [40] Penrose R 1969 Gravitational collapse: the role of general relativity *Riv. Nuovo Cimento* **1** special number 252-276
- [41] Krivan W, Laguna P, Papadopoulos P and Andersson N 1997 Dynamics of perturbations of rotating black holes *Phys. Rev. D* **56** 3395
- [42] Andersson N, Laguna P and Papadopoulos P 1998 Dynamics of Perturbations of Rotating Black Holes. II. A note on superradiance *Phys. Rev. D* **58** 087503
- [43] Starobinskii A A 1973 Amplification of waves during reflection from rotating "black hole" *Zh. Eksp. Teor. Fiz.* **64** 48-57
- [44] Finster F, Kamran N, Smoller J and Yau S T 2009 A rigorous treatment of energy extraction from rotating black hole *Commun. Math. Phys.* **287** 829-847
- [45] Dafermos M and Rodnianski I 2010 The black hole stability problem for linear scalar perturbations *Preprint* gr-qc/1010.5137
- [46] Messiah A 1961 Quantum mechanics I. (Amsterdam: North-Holland Publ. Comp.)
- [47] Genz A and Malik A 1980 An adaptive algorithm for numerical integration over an n-dimensional rectangular region *J. Comp. Appl. Math.* **6** 295
- [48] Price R H 1972 Nonspherical perturbations of relativistic gravitational collapse 1. scalar and gravitational perturbations *Phys. Rev. D* **5** 2419
- [49] Price R H 1972 Nonspherical perturbations of relativistic gravitational collapse 2. integer-spin, zero-rest-mass fields *Phys. Rev. D* **5** 2439
- [50] Adams R A 1975 Sobolev spaces (Academic Press)
- [51] Aubin T 1998 Some nonlinear problems in riemannian geometry (Springer)
- [52] Slater C 1960 Quantum theory of atomic structure (McGraw-Hill)
- [53] Gaunt J A 1929 On the triplets of helium *Philos. Trans. Roy. Soc. A* **228** 151
- [54] Messiah A 1962 Quantum Mechanics (North-Holland)
- [55] The GNU Scientific Library  
<http://www.gnu.org/software/gsl>
- [56] László A 2006 A robust iterative unfolding method for signal processing *J. Phys. A* **39** 13621
- [57] Aronszajn N 1950 Theory of reproducing kernels *Transactions of the American Mathematical Society* **68** 337